AFRL-AFOSR-VA-TR-2021-0024

High Power Recirculating Planar Amplifiers

Gilgenbach, Ronald
REGENTS OF THE UNIVERSITY OF MICHIGAN
503 THOMPSON ST
ANN ARBOR, MI,
US

04/07/2021
Final Technical Report

DISTRIBUTION A: Distribution approved for public release.

Air Force Research Laboratory
Air Force Office of Scientific Research
Arlington, Virginia 22203
Air Force Materiel Command

REPORT DOCUMENTATION PAGE	*Form Approved* *OMB No. 0704-0188*

1. REPORT DATE *(DD-MM-YYYY)*	**2. REPORT TYPE**	**3. DATES COVERED** *(From - To)*
07-04-2021	Final	01 Mar 2015 - 31 Aug 2020

4. TITLE AND SUBTITLE
High Power Recirculating Planar Amplifiers

5a. CONTRACT NUMBER

5b. GRANT NUMBER
FA9550-15-1-0097

5c. PROGRAM ELEMENT NUMBER

6. AUTHOR(S)
Ronald Gilgenbach

5d. PROJECT NUMBER

5e. TASK NUMBER

5f. WORK UNIT NUMBER

7. PERFORMING ORGANIZATION NAME(S) AND ADDRESS(ES)
REGENTS OF THE UNIVERSITY OF MICHIGAN
503 THOMPSON ST
ANN ARBOR, MI
US

8. PERFORMING ORGANIZATION REPORT NUMBER

9. SPONSORING/MONITORING AGENCY NAME(S) AND ADDRESS(ES)
AF Office of Scientific Research
875 N. Randolph St. Room 3112
Arlington, VA 22203

10. SPONSOR/MONITOR'S ACRONYM(S)
AFRL/AFOSR RTB1

11. SPONSOR/MONITOR'S REPORT NUMBER(S)
AFRL-AFOSR-VA-TR-2021-0024

12. DISTRIBUTION/AVAILABILITY STATEMENT
A Distribution Unlimited: PB Public Release

13. SUPPLEMENTARY NOTES

14. ABSTRACT
A novel high power (5-10 MW) crossed-field amplifier (RPCFA) based on the Recirculating Planar Magnetron concept invented at the University of Michigan has been designed and tested. Using computational modeling tools such as HFSS and MAGIC, a 3.0 GHz amplifier design has been modeled with 13.5 dB of gain (29 MW output). In simulation, the amplifier is zero-drive stable and exhibits greater than 50% electronic efficiency, not accounting for electron end-loss; or 15% including end-loss. This RPCFA
design was fabricated, constructed, and experimentally demonstrated, exhibiting amplification between 2.4 and 3.05 GHz, with peak powers up to 5-6 MW at peak gain of 8-10 dB. Maximum microwave output power is limited by RF breakdown in the slow-wave structure, which occurs between 3-6 MW. Amplifier gain exhibits improved reproducibility above 350 kW input microwave power. The RPCFA also demonstrated zero drive stability in experiments, up to 10 kA of injected current. Collaborations with AFRL explored the Recirculating Planar Magnetron with Coaxial-All-Cavity Extraction (RPM-CACE). This device was fabricated by AFRL and initial experiments have been performed at UM.
Preliminary experiments with moderate currents from bare metal cathodes have been promising, with total microwave power from all 6-waveguides of some 40 MW. Higher microwave power is expected with higher-current, carbon fiber cathodes presently being fabricated by AFRL. Another collaboration with AFRL concerned a theoretical study of the sinewaveguide traveling wave tube (TWT). Theoretical research has discovered a new space charge parameter, q, which describes the modification of the slow-wave circuit mode. This q is analogous to Pierce's original space charge parameter, Q, which describes the modification of the beam mode. This represents a major advancement
of Pierce's theory of traveling wave tube amplifier, which has been utilized for some 70 years in various forms. The exact formulation that led to the discovery of q also led to modification of Pierce's gain parameter C and of the Pierce's space charge parameter Q. More recently, the investigators extended the theory to include the modification of the last Pierce's parameter, the loss parameter, d, that accounts all cold-tube circuit loss. In this sense, the modification of Pierce's classical TWT theory is complete.
Other TWT theoretical issues were studied for the first time, including novel harmonic generation mechanisms, absolute instability at the band edges and their temporal evolution, and backward wave oscillations in the presence of random manufacturing error or errors.

15. SUBJECT TERMS

16. SECURITY CLASSIFICATION OF:			**17. LIMITATION OF ABSTRACT**	**18. NUMBER OF PAGES**	**19a. NAME OF RESPONSIBLE PERSON**
a. REPORT	**b. ABSTRACT**	**c. THIS PAGE**			JULIE MOSES
U	U	U	UU	40	**19b. TELEPHONE NUMBER** *(Include area code)* 426-9586

AFOSR Final Performance Report

"High Power Recirculating Planar Amplifiers"

Award #: FA9550-15-1-0097

Performance Period: March 1, 2015 – August 30, 2020

AFOSR Program Manager:
Dr. Ali Sayir
Air Force Office of Scientific Research
875 N. Randolph St.
Arlington, VA 22203

Principal Investigator:
Prof. Ronald Gilgenbach
rongilg@umich.edu
(734) 763-1261
Co-Principal Investigators
Prof. Y.Y. Lau
yylau@umich.edu
(734) 764-5122
Dr. Nicholas Jordan
jordann@umich.edu
(734) 763-0213
Nuclear Engineering and Radiological Science Department
University of Michigan
2355 Bonisteel Blvd.
Ann Arbor, MI 48109
Period of performance:
March 1, 2015-August 31, 2020

November 2020

Summary

A novel high power (5-10 MW) crossed-field amplifier (RPCFA) based on the Recirculating Planar Magnetron concept invented at the University of Michigan has been designed and tested. Using computational modeling tools such as HFSS and MAGIC, a 3.0 GHz amplifier design has been modeled with 13.5 dB of gain (29 MW output). In simulation, the amplifier is zero-drive stable and exhibits greater than 50% electronic efficiency, not accounting for electron end-loss; or 15% including end-loss. This RPCFA design was fabricated, constructed, and experimentally demonstrated, exhibiting amplification between 2.4 and 3.05 GHz, with peak powers up to 5-6 MW at peak gain of 8-10 dB. Maximum microwave output power is limited by RF breakdown in the slow-wave structure, which occurs between 3-6 MW. Amplifier gain exhibits improved reproducibility above 350 kW input microwave power. The RPCFA also demonstrated zero-drive stability in experiments, up to 10 kA of injected current.

Collaborations with AFRL explored the Recirculating Planar Magnetron with Coaxial-All-Cavity Extraction (RPM-CACE). This device was fabricated by AFRL and initial experiments have been performed at UM. Preliminary experiments with moderate currents from bare metal cathodes have been promising, with total microwave power from all 6-waveguides of some 40 MW. Higher microwave power is expected with higher-current, carbon fiber cathodes presently being fabricated by AFRL. Another collaboration with AFRL concerned a theoretical study of the sine-waveguide traveling wave tube (TWT).

Theoretical research has discovered a new space charge parameter, *q*, which describes the modification of the slow-wave circuit mode. This q is analogous to Pierce's original space charge parameter, Q, which describes the modification of the beam mode. This represents a major advancement of Pierce's theory of traveling wave tube amplifier, which has been utilized for some 70 years in various forms. The exact formulation that led to the discovery of q also led to modification of Pierce's gain parameter C and of the Pierce's space charge parameter Q. More recently, the investigators extended the theory to include the modification of the last Pierce's parameter, the loss parameter, *d*, that accounts all cold-tube circuit loss. In this sense, the modification of Pierce's classical TWT theory is complete. Other TWT theoretical issues were studied for the first time, including novel harmonic generation mechanisms, absolute instability at the band edges and their temporal evolution, and backward wave oscillations in the presence of random manufacturing errors.

Table of Contents

Table of Figures

Introduction

This research program was directed towards the goal of a high power (5-10 MW) crossed-field amplifier (RPCFA) based on the Recirculating Planar Magnetron concept invented at the University of Michigan. Using computational modeling tools such as HFSS and MAGIC, a 3.0 GHz amplifier design with 13.5 dB of gain (29 MW output) has been modeled. In simulation, the amplifier is zero-drive stable and exhibits greater than 50% electronic efficiency, not accounting for electron end-loss; 15% including endloss current. This RPCFA design has been fabricated, constructed, and experimentally demonstrated, exhibiting amplification between 2.4 and 3.05 GHz, with peak powers up to 5-6 MW at peak gain of 8-10 dB. Maximum microwave output power is limited by RF breakdown in the slow wave structure, which occurs between 3-6 MW. Amplifier gain exhibits improved reproducibility above 350 kW input microwave power. The RPCFA has also demonstrated zero-drive stability in experiments, up to 10 kA of injected current.

Collaborations with AFRL also explored the Recirculating Planar Magnetron with Coaxial-All-Cavity Extraction (RPM-CACE). This device was fabricated by AFRL and initial experiments have been performed at UM. Preliminary experiments with low currents from bare metal cathodes have been promising, with total microwave power from all 6-waveguides of some 40 MW. Higher microwave power is expected with carbon fiber cathodes presently being fabricated by AFRL.

Theoretical research has discovered a new space charge parameter, *q*, that describes the modification of the slow-wave circuit mode. This q is analogous to Pierce's original space charge parameter, Q, which describes the modification of the beam mode. This represents a major advancement of Pierce's theory of traveling wave tube amplifier, which has been utilized for some 70 years in various forms. The exact formulation that led to the discovery of q also led to modification of Pierce's gain parameter C and of the Pierce's space charge parameter Q. More recently, the investigators extended the theory to include the modification of the last Pierce's parameter, the loss parameter, *d*, that accounts all cold-tube circuit loss. In this sense, the modification of Pierce's classical TWT theory is complete. Also studied are various theoretical issues in TWT, including the backward wave oscillations in the presence of random manufacturing errors, novel mechanisms for harmonic generation, band-edge oscillations, and a novel sine-waveguide TWT originated from the Air Force Research Laboratory. The stability in the Brillouin flow in crossed-field devices are studied for the first time that explicitly included the slow wave structure.

Much of the work described herein was included in recent University of Michigan Ph.D. dissertations funded by this grant [1,2]. An additional dissertation expanding the analytic theory will be completed early in 2021.

---

[1] P. Y. Wong, "A Contemporary Study in the Theory of Traveling-Wave Tubes," doctoral dissertation, University of Michigan, Ann Arbor, MI, 2018.
[2] S.C. Exelby, "Design, Development, and Experiments on the Recirculating Planar Crossed Field Amplifier" doctoral dissertation, University of Michigan, Ann Arbor, 2019.

Methods, Assumptions, and Procedures

Analytic Theory

Backward wave oscillations in a TWT

Backward wave oscillation (BWO) poses a serious threat to the stable operation of a traveling-wave tube (TWT). The threshold for the onset of BWO in a TWT was formulated by Johnson. We extended Johnson's model to include random variations of circuit phase velocity along the tube axis (Figure 1). We also include the effects of end reflections. This work was in part motivated by a test experimental helix TWT in which BWO was not observed even though it was predicted to occur according to the classical Johnson theory [3].

When random variations in the Pierce's detune parameter *b* (circuit phase velocity) occur along the TWT (Figure 1), the classical 3-wave theory of Pierce is governed by the non-dimensional differential equation [4],

$$\frac{d^3 f(x)}{dx^3} + jC(b + jd)\frac{d^2 f(x)}{dx^2} + C^2(4QC)\frac{df(x)}{dx} + jC^3\,(4QC(b + jd) - 1)f(x) = 0 \tag{1}$$

where C, QC, b, and d, are Pierce's parameters measuring the gain, the effects of AC space charge, circuit detune, and circuit loss, respectively. One thousand cases of such random samples of b were run, each of which was applied to Eq. (1). The statistical distribution of the threshold value of Pierce's gain parameter C for the onset of BWO is shown in Figure 2 for these 1000 cases, setting d = 0, and QC = 0. Here we see that the BWO threshold was only minimally affected by random variations in the phase velocity. This relative insensitivity of Johnson's BWO threshold is likely due to the cancellation of all three waves at z = L (Figure 1) and therefore the sensitivity of b that characterizes synchronous interaction is of lesser importance. The effect of nonzero QC is shown in Figure 3, which shows that the value of threshold C increases by 50 percent as QC increases from 0 to 1.

We next assume that the circuit parameters are uniform, but we include finite reflections of the backward (forward) circuit wave at z = 0 (z = L) with composite reflection coefficient $\mathrm{R}e^{j\phi}$. Figure 4 shows the significant effects of R and ϕ on the threshold gain parameter, CN. A nonzero R lowers the threshold CN in general. Our generalization of Johnson's theory did not explain why an L-3 Communications helix TWT did not oscillate even though the Pierce parameter *CN* in the experiment exceeded the theoretical threshold value. One reason, we suspect, is that the values of *QC*, *d*, the reflection coefficients, and/or the beam radius required for application of Johnson's theory may not be known with sufficient accuracy [3].

---

[3] A. Jassem, P. Y. Wong, D. P. Chernin, Y. Y. Lau, F. Antoulinakis, T. A. Hargreaves and C. M. Armstrong, "On Johnson's Backward Wave Oscillation Thresholds in TWT," in *2018 IEEE Int. Vacuum Electronics Conference (IVEC)*, Monterey, CA, USA, 2018 pp. 171-172.

[4] Abhijit Jassem, Patrick Y. Wong, David P. Chernin, Y. Y. Lau, Foivos Antoulinakis, Drew Packard, Thomas A. Hargreaves and Carter M. Armstrong, "Extensions of Johnson's theory of backward wave oscillations in traveling wave tubes," IEEE Trans. Electron Devices (January, 2019).

Figure 1: Example of random variation along tube axis; b is Pierce's detune parameter [4].

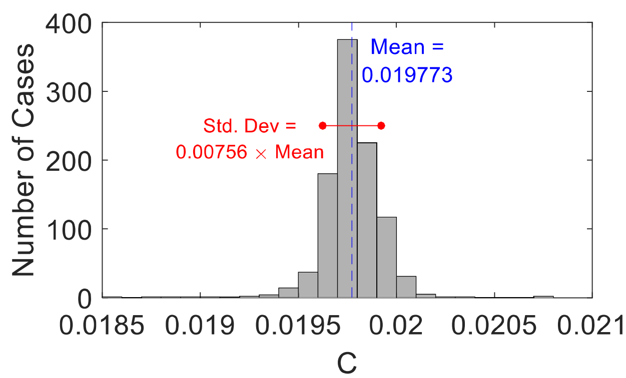

Figure 2: Distribution in threshold Pierce gain parameter C for standard deviation in detune parameter $\sigma_b = 1.7$ (corresponding to standard deviation in circuit phase velocity of 3.4 percent). Here, $QC = 0$, $d = 0$ [4].

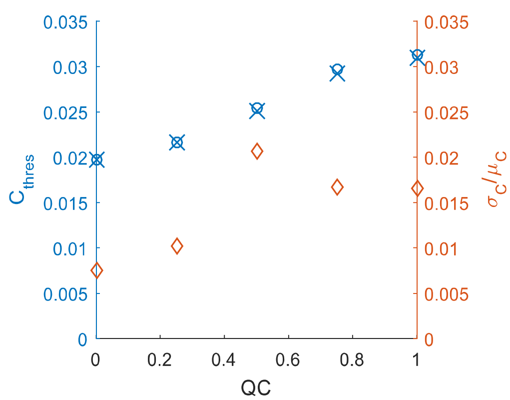

Figure 3: Means and relative standard deviations of gain parameter as a function of QC. Here, d = 0 [4].

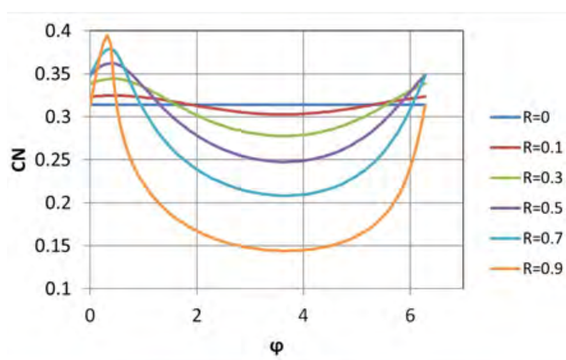

Figure 4: Effects of end reflections on the threshold gain parameter CN. Here, QC=0, d=0 [4].

Modification of Pierce's classical TWT theory

This is an important accomplishment. Pierce's classical theory of TWT laid the foundation for the generation of coherent radiation from the interaction of an electron beam with a periodic structure. The weakest aspect of this theory of mode coupling concerns the modification of the beam mode at high beam currents; this modification was characterized by Pierce's space-charge parameter, *Q*, for which no general calculation was given. An accurate determination of *Q* is important for at least three reasons: first, a small discrepancy in *Q* can lead to a large change in the predicted small-signal gain. Second, an accurate value of *Q* (or *QC*) is required by the nonlinear TWT simulation codes such as CHRISTINE in order to compute large-signal quantities like saturated output power and efficiency. Third, in Johnson's classical theory for the onset of backward wave oscillations in TWT, the threshold conditions depend only on *QC* and on *d*, Pierce's loss parameter, which implies that prediction of BWO threshold current requires accurate values of *QC* and *d*. See Figure 3 above.

For a realistic case of an electron beam interacting with the electromagnetic fields supported by a thin perfectly conducting tape helix (Figure 5), we derive the exact dispersion relation [5],

$$[(\beta-\beta_e)^2-4\beta_e^2QC^3]\left[\left(\beta-\beta_{ph}\right)-4\beta_{ph}qC^3\right]=-\beta_e^3C^3 \qquad (2)$$

where q is a new parameter introduced to account for the space-charge effect on the circuit mode. In Eq. (2), β is the complex wavenumber for signal frequency ω , $\beta_e=\omega/v_0$, $\beta_{ph}=\omega/v_{ph}$, v_0 is the DC beam velocity, and v_{ph} is the phase velocity of the circuit wave on the cold-tube circuit. Note from Eq. (2) that *q* produces a circuit phase velocity change due to a space-charge effect, by a fraction equal to $4qC^3$. This new parameter, *q*, is introduced by the investigators [1, 5] for the first time in the literature of TWT. Physically, Eq. (2) describes the modification of the beam mode at high current through *Q*, and the modification of the cold-tube circuit mode through *q*. In the realistic example (Figure 5), we find that $4qC^3$ = 4*5*0.1^3 = 0.02 (Figure 6), which is equivalent to a two percent detune in the circuit - a very significant effect.

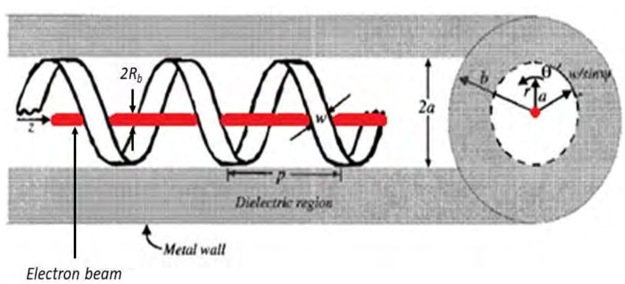

Figure 5: Schematic diagram of tape helix TWT model [5].

[5] P.Y. Wong, D. Chernin, and Y.Y. Lau, "Modification of Pierce's Classical Theory of Traveling-Wave Tubes," IEEE Electr. Dev. Lett. 39 1238-1241 (2018).

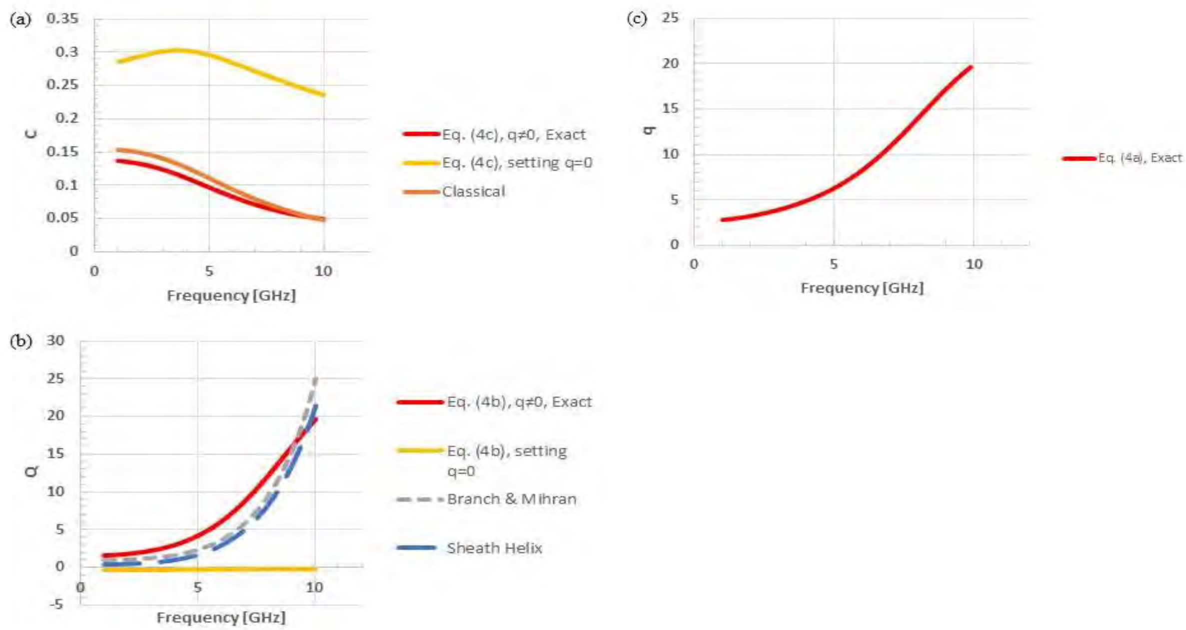

Figure 6: Plots of the exact Pierce parameters [(a) C, (b) Q, (c) q] and their traditional definitions as a function of frequency [5].

We then further extended our modification of Pierce's classical TWT dispersion relation to include realistic cold-tube loss. As noted above, we found the surprising results that Pierce's classical theory of traveling-wave tube (TWT) requires revision at a high electron beam current because of space charge effects [5]. A new space charge parameter, q, was discovered that describes the modification of the circuit mode. It is analogous to Pierce's original space charge parameter, Q, which describes the modification of the beam mode. This theory assumes that the circuit is lossless.

Including cold tube circuit loss, which is always present in a real tube, we propose that the classical Pierce 3-wave dispersion relation for TWT is modified to read [6],

$$[(\beta-\beta_e)^2 - 4\beta_e^2 Q C^3][\beta-\beta_p-4\beta_p q C^3 + jCd\beta_e] = -\beta_e^3 C^3 \qquad (3)$$

In Eq. (3), β is the propagation constant at frequency ω, $\beta_e = \omega/v_o$, $\beta_p = \omega/v_p$, v_0 is the beam velocity, v_p is the phase velocity of the forward circuit wave, *Q*, *q*, and *C* (= Pierce's gain parameter) are determined exactly *as if the circuit were lossless*, as in [5], and *d* is Pierce loss parameter associated with the cold tube loss. Equation (1) has three attractive properties: (a) the parameters Q, *q*, and *C* are all real because they were derived assuming *d* = 0, (b) It reduces to [5] when *d* = 0, where the parameters Q and C are different from that of Pierce's classical values, because Pierce employed only the dominant cold-tube circuit mode, whereas we determined Q and *C* using our exact theory which included all hot-tube circuit modes, and

[6] A. Jassem, Y. Y. Lau, D. P. Chernin, and P. Wong, "Theory of traveling wave tube including space charge effects on the circuit mode and distributed cold tube loss," IEEE Transactions on Plasma Science 48, 665-668 (2020).

(c) Eq. (3) reduces to the form of Pierce's classical theory for a lossy tube when q = 0 (though, again, not the values of Q and C).

In Figure 7, we show the differences in C, QC, and d between our "exact" theory and Pierce's classical theory (labelled "Pierce"), for a tape helix TWT model driven by a 3 kV, 0.17 A pencil e-beam of beam radius 0.05 cm [5]. The small signal gain for such a (uniform) tube with interaction length $L = 10$ cm is plotted in Figure 8. The exact and Pierce theory agree well only in a restricted frequency range, and significant divergence is observed below 4 GHz and above 8 GHz. This is most likely attributed to the discrepancy in the same frequency range in C and in *d* (Figure 7).

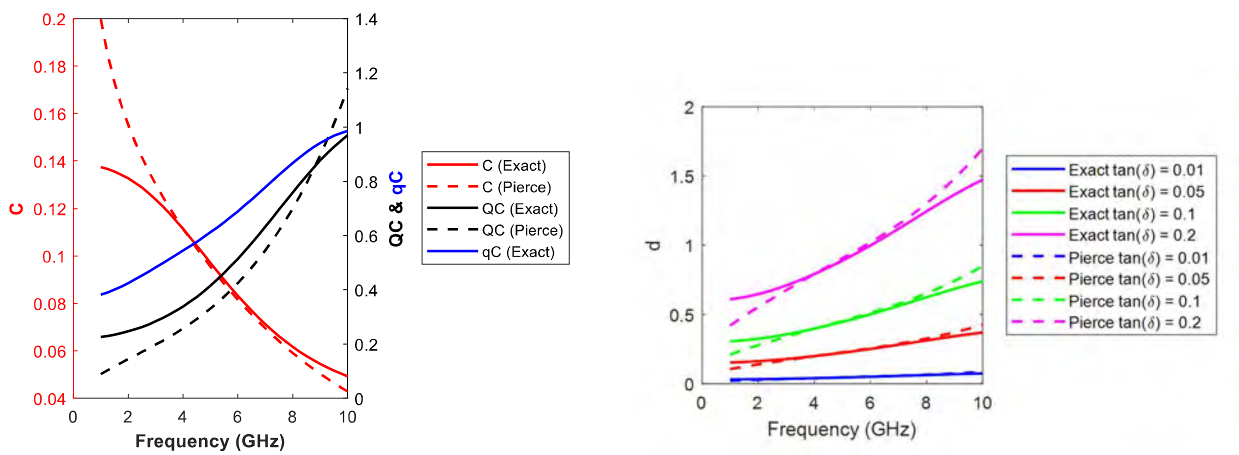

Figure 7: Plots of Pierce parameters (a) left, C, QC, and qC for d=0; (b) right, d from the exact solution and the classical Pierce approach, at various loss tangents [6].

We next consider two realistic test cases of TWTs with severs [6]; one has uniform attenuation while the other has a variable attenuation profile. Fixing the frequency at 4.5 GHz, Figure 9 shows general agreement between the exact and Pierce theory over the length of the tube, although significant divergence is observed immediately after the sever. This discrepancy is due to the detuning effect of q, although Q is compensated which leads to good agreement between the two solutions (see Figure 7a).

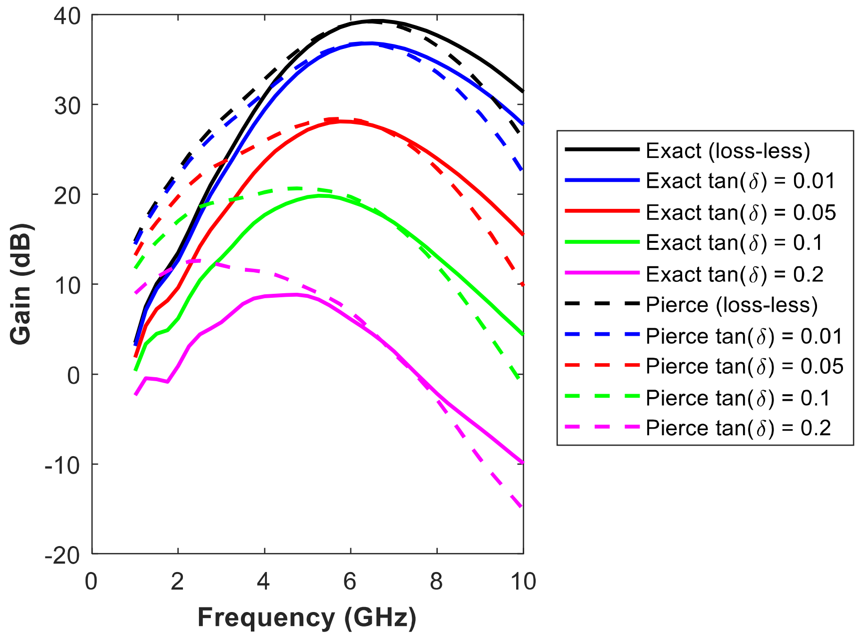

Figure 8: Gain for a TWT of interaction length L= 10 cm from exact and Pierce solutions [6].

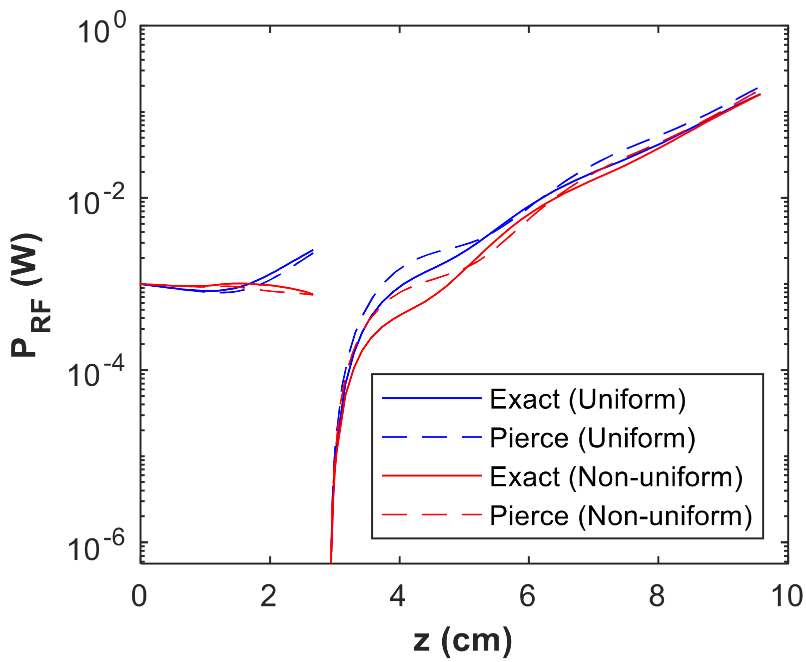

Figure 9: RF power profile for the Pierce and Exact cases using the uniform and non-uniform attenuation profiles at 4.5 GHz with input power of 1 mW. The sever is between z = 2.667 cm and z = 2.921 cm [6].

Stability of Brillouin Flow for Conventional and Inverted Magnetrons

For the first time [7], we contrast the stability of Brillouin flow in the conventional and inverted magnetron geometry, including a slow wave structure (SWS) on the anode (Figure 10). The Brillouin flow is the prevalent flow in crossed-field devices. This is particularly important because three major effects came into play which were never analyzed simultaneously: (a) the diocotron instability associated with the shear flow, (b) the positive (negative) mass effect that accompanies the conventional (inverted) magnetron geometry, and (c) the synchronous interaction between the SWS with the combined instabilities in (a) and (b).

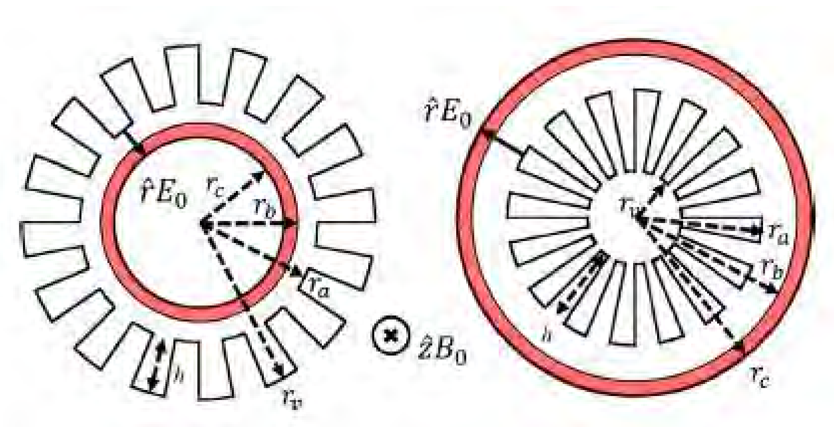

Figure 10: Geometry of conventional (left) and inverted (right) cylindrical magnetrons [7].

Our formulation is fully relativistic and fully electromagnetic, and it incorporates the equilibrium density profile, flow profile, electric field and magnetic field profiles in the linear stability analysis [7,8]. To have a fair comparison between the two cases, we use parameters similar to our experiments on the recirculating planar magnetron, as shown in Table 1. The result of the linear stability analysis is shown in Figure 11 [7].

[7] D. H. Simon, Y. Y. Lau, G. Greening, P. Wong, B. Hoff, and R. M. Gilgenbach, "Stability of Brillouin flow in the presence of slow-wave structure," Phys. Plasmas. **23**, 092101 (2016).
[8] D. H. Simon, "Equilibrium and Stability of Brillouin Flow in Planar, Conventional, and Inverted Magnetrons", PhD dissertation, University of Michigan, Ann Arbor (2016).

Table 1: Operational parameters and geometry for the base case conventional and inverted magnetrons. Quantities that are the same between the two types and the planar magnetron are highlighted in bold. The highlighted parameters are similar to the RPM experiments at the University of Michigan.

Parameter	Conventional	Inverted
Cathode radius: r_c	10 cm	13.9 cm
Anode radius: r_a	13.9 cm	10 cm
AK gap: $\lvert r_c - r_a \rvert$	**3.9 cm**	**3.9 cm**
Brillouin hub: $\lvert r_b - r_c \rvert$	**1.54 cm**	**1.54 cm**
$h : \lvert r_v - r_a \rvert$	**6.31 cm**	**6.31 cm**
Magnetic field: B_0	**0.0645 T**	**0.0645 T**
Applied voltage: V	238 kV	378 kV
Number of cavities: N	16	16

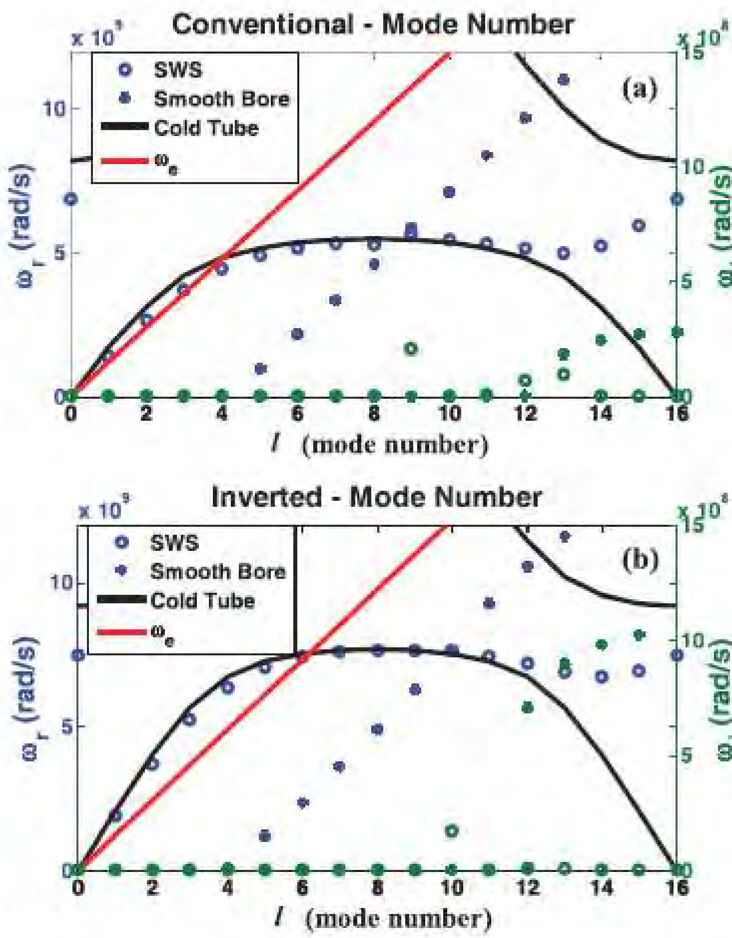

Figure 11: Eigenvalue and cold tube solutions, along with the beam line ω_e, for (a) conventional and (b) inverted cylindrical magnetron for ω_r and ω_i as a function of the azimuthal mode number l, with all other parameters equal to the base case. Circular markers correspond to SWS, plus sign markers to smooth-bore. The filled circles are intersections of the empty circles and the plus sign markers and indicate that the SWS and smooth-bore frequencies are the same for that mode [7].

The numerical data show the following novel results. The resonant interaction of the vacuum circuit mode and the corresponding smooth-bore diocotron-like mode is the dominant cause for instability in Brillouin flow in the conventional and inverted magnetron geometry that include a slow wave structure on the anode. This resonant interaction is far more important than the intrinsic negative (positive) mass property of electrons in the inverted (conventional) magnetron geometry. It is absent in either the smooth-bore magnetron, or under the electrostatic assumption, one or both of which was almost always adopted in prior analytical formulation. This resonant interaction severely restricts the wavenumber for instability to the narrow range in which the cold tube frequency of the SWS is within a few percent of the corresponding smooth bore diocotron-like mode in the Brillouin flow [7,8].

Analysis of a sine-waveguide TWT

We have collaborated with AFRL colleagues [9] to investigate the viability of a 20-stage X-band sine waveguide amplifier, driven by a cylindrical electron beam (Figure 12). This geometry is simpler to fabricate than the coupled-cavity TWT, even though the latter tends to produce the highest output power.

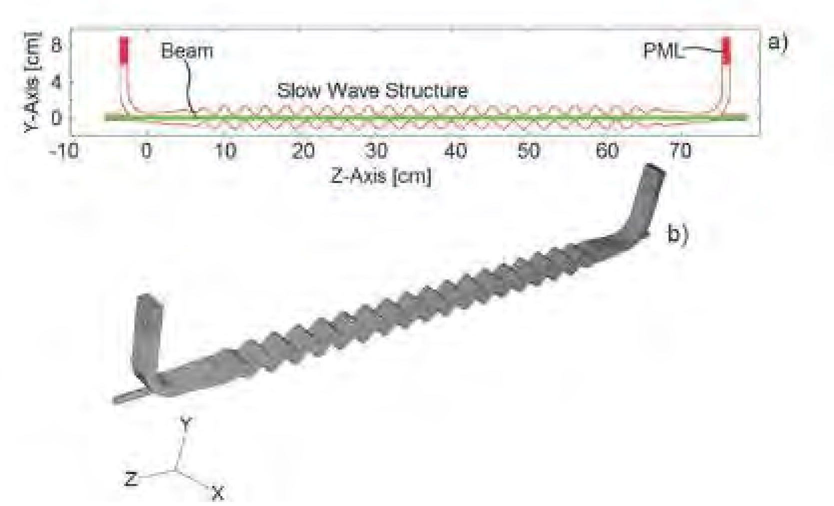

Figure 12: a) 2-D cross section geometry of the simulated sine waveguide TWT. b) 3-D mesh plot example of a simulated sine waveguide TWT geometry (the displayed TWT mesh plot is 5 periods shorter than the simulated device used in this study for a better aspect ratio in the figure) [9].

The complicated geometry shown in Figure 12 prevents any realistic assessment of the conventional Pierce's parameters C, b, QC, and d, which, respectively, characterize the TWT gain, detune, “space charge effect”, and cold-tube circuit loss. From the AFRL simulation, we were able to give a very rough estimates of these parameters, as shown in Figure 13.

[9] Brad W. Hoff, David S. Simon, David M. French, Y. Y. Lau, and Patrick Wong, "Study of a high power sine waveguide traveling wave tube amplifier centered at 8 GHz," Phys. Plasmas **23**, 103102 (2016).

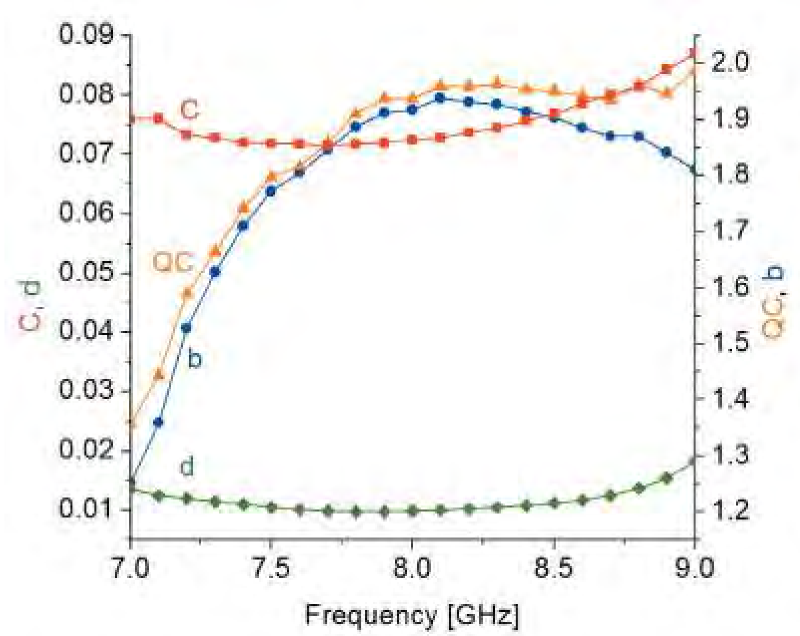

Figure 13: Values of C, b, and d for a sine-waveguide TWT driven by a 40 A, 100 kV pencil beam. The interaction impedance and circuit phase velocity used in C and b were obtained from HFSS. Also shown are the values of QC required to match the 1.8 kW input power level case with Pierce's 3-wave TWT theory [9].

In an earlier attempt [10], we studied an exactly solvable model of a traveling wave tube (TWT) to show that Pierce gain parameter C and space charge parameter Q generally depend on wavenumber k in addition to frequency ω. The choice of k at which C and Q are evaluated may strongly affect their values and, consequently, the values of the small signal gain obtained from 3- and 4- wave Pierce theory. In order to illustrate this effect, we calculate the spatial amplification rate, k_i, from the exact dispersion relation for a dielectric TWT model which is exactly solvable. We compare this exact value of k_i with approximate values obtained from Pierce's classical 3-wave and 4-wave dispersion relations, obtained by making various assumptions on k in the evaluation of C and Q. We find that the various ways to approximate C and Q will have a significant influence on the numerical values of k_i. For our dielectric TWT example, Pierce's 4-wave TWT dispersion relation generally yields the most accurate values of k_i if Q is evaluated for $k=\omega/v_0$, where v_0 is the beam velocity, and if the complete frequency and wavelength dependence of C is retained. Pierce's 3-wave theory also yields accurate values of k_i using a different form of Q from the 4-wave theory. The implications of this result for TWT design are explored [10].

Harmonic generation in a TWT

A well-known non-linear process in vacuum electronics that leads to harmonic beam current, due to an input signal of a single frequency, ω_0, is crowding of the electron orbits, in which neighboring electrons are getting closer together. This orbital crowding produces a rather high

[10] D. H. Simon, P. Wong, D. Chernin, Y. Y. Lau, B. Hoff, P. Zhang, C. F. Dong, and R. M. Gilgenbach, " On the evaluation of Pierce parameters C and Q in a traveling wave tube," Phys. Plasmas **24**, 033114 (2017).

second harmonic AC current in the beam in a TWT, reaching 1/4 of the DC beam current [11], even though the electron's AC velocity is in the *linear* regime (as in the klystron analysis).

We discovered another source of harmonic current, which is far more important than that due to orbital crowding that was described in the preceding paragraph. This harmonic current is due to the non-linear correction in the electron orbit, which is described by the non-linear convective derivative in the force law, $v_1 \frac{\partial v_1}{\partial z}$, where $v_1 = v_{10} e^{j\omega_0 t - jk_0 z}$ is the linearized electron fluid velocity at the fundamental frequency (ω_0), whose wavenumber $k_0 \approx \frac{\omega_0}{v_0}$ where v_0 is the DC beam velocity. This convective derivative, $v_1 \frac{\partial v_1}{\partial z}$, then contributes a "force" proportional to $v_{10}^2 e^{j2\omega_0 t - j2k_0 z}$. This "force" is a traveling wave at the second harmonic frequency. It has a phase velocity also synchronized with the electron beam because $\frac{\omega}{k} = \frac{2\omega_0}{2k_0} = \frac{\omega_0}{k_0} \approx v_0$. This "force" may then synchronously excite a second harmonic wave, both in time and space, which makes it a much more powerful contributor to second harmonic generation. The AC harmonic current due to orbital crowding, described in the preceding paragraph, does not possess this property of synchronization in both time and space, and is therefore a much weaker contributor in the generation of RF power at the second harmonic. This is a rather unexpected finding [12], because we did not anticipate that the non-linear term $v_1 \frac{\partial v_1}{\partial z}$ would be so important, as v_1 is admittedly in the linear regime. Comparison with CHRISTINE simulation confirmed these facts, as shown in Figure 14.

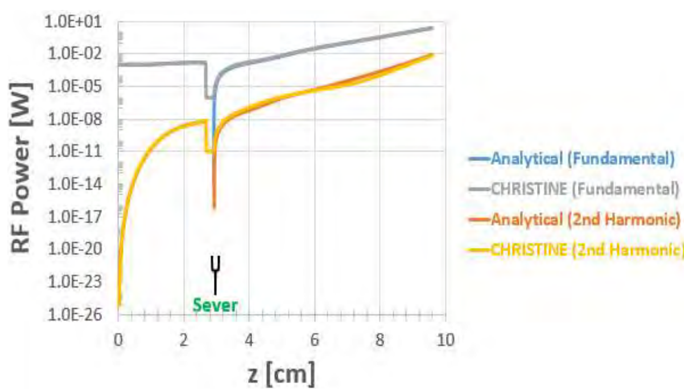

Figure 14: The RF power profile at fundamental and second harmonic for a realistic TWT test case that includes distributed circuit loss and a narrow sever region [12].

Absolute instability at the TWT band edges

TWTs are known to be subjected to absolute instability when the beam mode intersects the circuit mode near the lower or the upper band edge, respectively labeled as Points A and B in Figure 15. These points have zero group velocity in the circuit mode. Absolute instability at

[11] C. F. Dong, P. Zhang, D. P. Chernin, Y. Y. Lau, B. W. Hoff, D. H. Simon, P. Wong, G. B. Greening, and R. M. Gilgenbach, “Harmonic Content in the Beam Current in a Traveling-Wave Tube,” *IEEE Transactions on Electron Devices*, Vol. 62, No. 12, p. 4285, December 2015.

[12] Patrick Y. Wong, Y. Y. Lau, David Chernin, Brad W. Hoff, and Ronald M. Gilgenbach, "Origin of Second Harmonic Signals in Octave Bandwidth Traveling-Wave Tubes," *IEEE Transactions on Electron Devices*, Vol. 65, No. 2, p. 720, February 2018.

these band edges have been studied using the Briggs-Bers criterion. Previous investigators have claimed that, for an operating point Q that lies between A and B (Figure 15), i.e., with a forward group velocity at Q, an absolute instability can occur only at the upper band edge, but not the lower band edge. Since the lower band edge was (erroneously) perceived as to be free of absolute instability, we attempted to assess the possible transient growth at the lower band edge. In this re-examination of the lower band edge, we discovered that the lower band edge does suffer from absolute instability when the beam current is sufficiently high. [13] Figure 16 shows that the threshold ε (which is proportional to the beam current) for the upper band edge is orders of magnitude smaller than it is for the lower band edge, for similar deviation of the operating point, Q, from points A and B in Figure 15. This implies that the upper band edge is significantly more prone to absolute instability than the lower band edge.

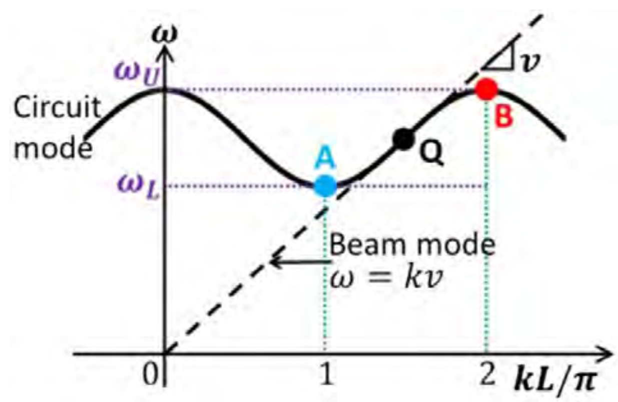

Figure 15: The lower band edge (A), the upper band edge (B), and the operating point (Q) at which the beam mode intersects with the circuit mode in a coupled cavity TW. kL is the phase shift per period [13].

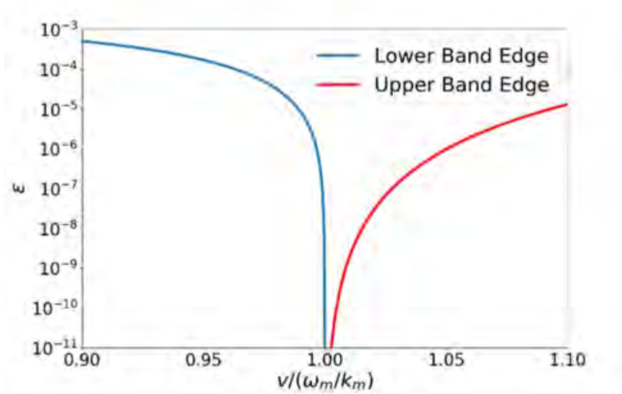

Figure 16: Threshold values of ϵ for lower band edge ($v < \omega_m/k_m$) and upper band edge ($v > \omega_m/k_m$). Here, ω_m/k_m is the circuit phase velocity at the corresponding band edge in Figure 15 [13].

When the TWT is not subjected to an absolute instability, an initial perturbation may still undergo transient growth (at a fixed position z) before the perturbation is convected away. The

[13] Foivos Antoulinakis, Patrick Wong, Abhijit Jassem, and Y. Y. Lau, “Absolute instability and transient growth near the band edges of a traveling wave tube” *Physics of Plasmas* **25**, 072102 (2018); doi: 10.1063/1.5028385

Green's function constructed from the dispersion relation near both band edges, A and B (Figure 15), indeed shows such a transient growth [13]. We express the magnitude of Green's function in exponential form, $\exp\left[k_m z f(T)\right]$, where $T = \frac{\omega_m t}{k_m z}$. Figure 17 shows the time dependence of *f*(*T*) for the lower band edge when it is stable, marginally stable, and unstable against absolute instability. In all three cases, $f(T) \sim T^{1/3}$, transiently (Figure 17). Our calculations of the Green's function have thus validated the stability criterion shown in Figure 17 [13]. They may well be the first explicit calculation of transient growth and its transition to the asymptotic behavior according to the Briggs-Bers criterion.

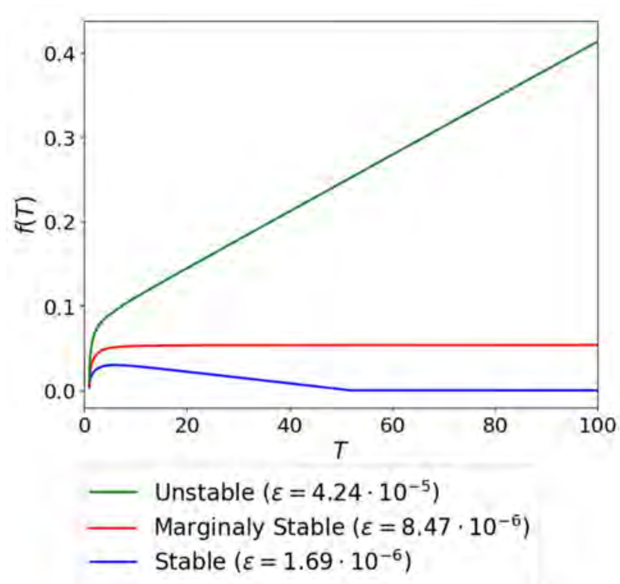

Figure 17: f(T) for the lower band edge with $v = 0.99\omega_m/k_m$. Note that ε is approximately equal to $2C^3$, where C is Pierce's gain parameter [13].

RPCFA Design and Simulation

The Recirculating Planar Crossed Field Amplifier (RPCFA) was based on the concept of the Recirculating Planar Magnetron (RPM), invented at UM during a previous AFOSR funded research effort. The RPCFA (Figure 18a) was expected to maintain many of the advantages of the RPM over traditional magnetrons and apply them to crossed-field amplifiers (CFAs) (Figure 18b). In the RPCFA, the amplifying section can easily be made longer or shorter, and the recirculating bends effectively demodulate the beam and minimizing feedback which may otherwise limit output power, giving the RPCFA some potential advantages over traditional CFAs.

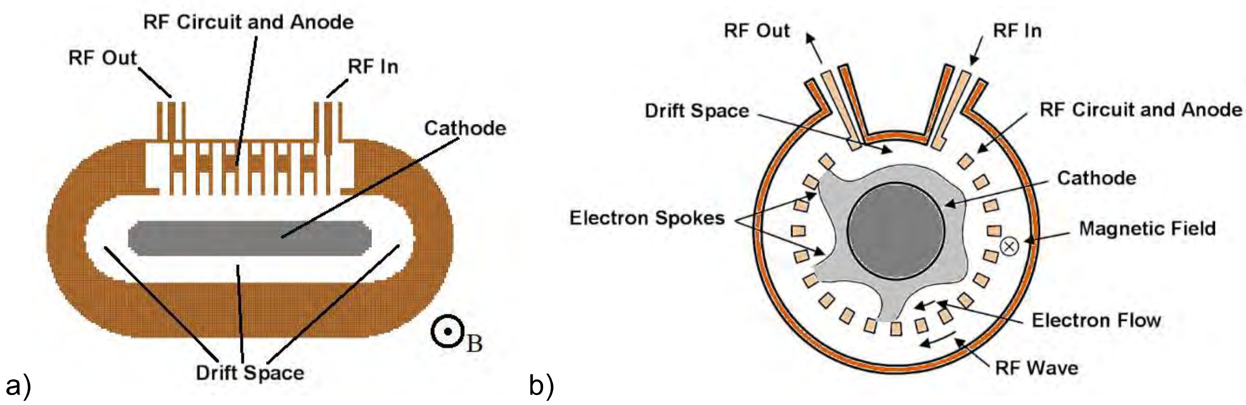

Figure 18: a) Potential RPCFA design. b) Common conventional CFA design.

Initial Recirculating Planar Crossed Field Amplifier (RPCFA) development work looked at several embodiments, including a single helix, folded waveguide, and double helix shown in Figure 19. Using the finite-element, frequency-domain code Ansys HFSS, and the time-domain, particle-in-cell code MAGIC developed by Alliant Techsystems (ATK), a RPCFA unit cell (the repeating element forming the slow wave structure) was constructed and iteratively simulated. The driven modal and eigenmode solvers of HFSS were used to determine the S-parameters and generate the dispersion relations for each cell. The dimensions of the slow wave structure were varied in order to establish a structure that supports the electric field geometry expected for an amplifier and minimize the potential for oscillation. The dispersion relations were generated to characterize the effect of a given parameter on the frequency and wavelength of the electric field.

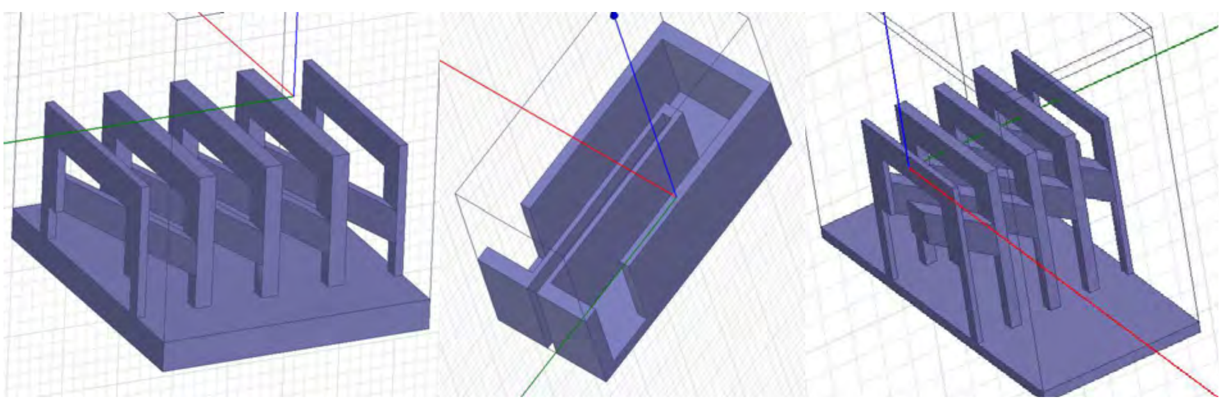

Figure 19: Single helix (left), folded waveguide (center), and double helix (right) slow wave structures simulated via unit-cell analysis in HFSS.

The goals for each design were: the structure must transmit a wave at the design frequency, 3 GHz, with minimal reflection at either end of the cell. The structure must also reduce the phase velocity of the 3 GHz wave to a value at which an electron hub may interact with, roughly 20% to 35% of the speed of light. Finally, the structure should minimize the possibility of exciting oscillations. Oscillatory modes can be found by analyzing the S-parameters and also by observing the dispersion relation. Once a design was found that satisfied these goals, the structure was built in MAGIC and run without particle emission to verify the HFSS generated dispersion relation and look for additional possible undesired modes of oscillation. Particle emission was then permitted, assuming agreement with HFSS, and the properties of the design such as gain, efficiency and spectrum were analyzed. The final slow wave structure (SWS) that emerged from this process is shown in Figure 20.

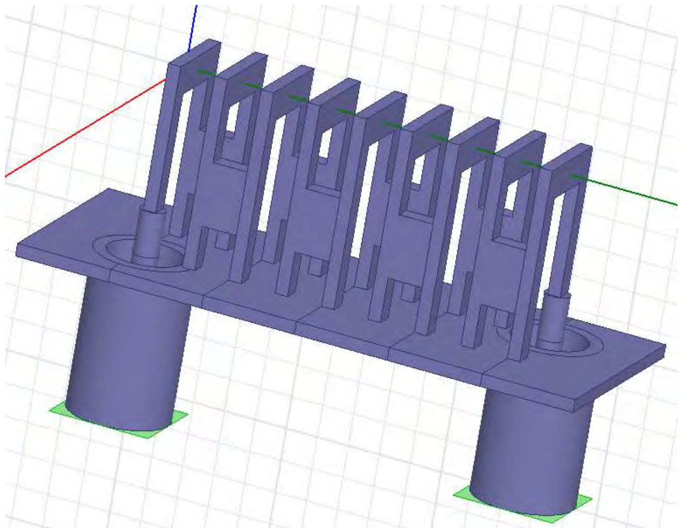

Figure 20: The RPCFA slow wave structure optimized in HFSS.

This SWS was fabricated from copper using 3D printing and a lost-wax casting process (Figure 21). This process was dramatically faster and orders of magnitude cheaper than conventional machining options. A full assembly including input and output couplers was designed and fabricated (Figure 22).

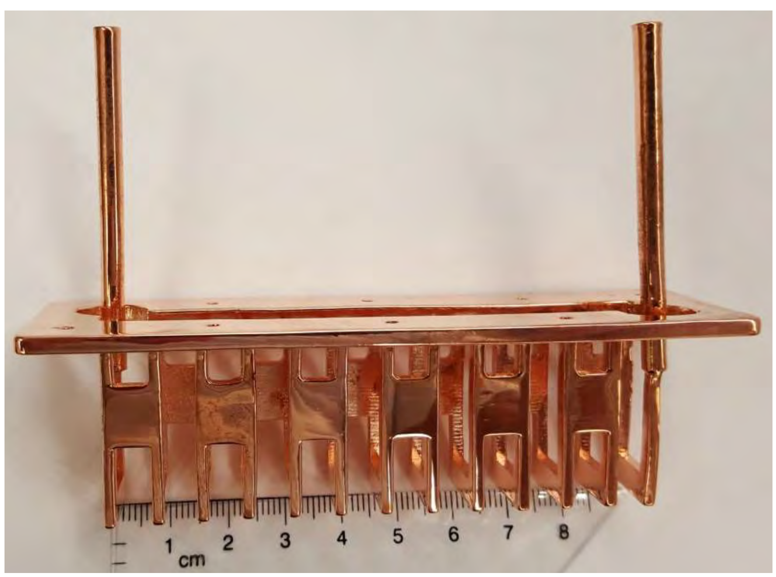

Figure 21: Additively manufactured copper slow wave structure, fabricated using 3D printing and a lost-wax casting process. This part is designed to slot into the larger anode structure, making electrical contact along the sides and bottom surface.

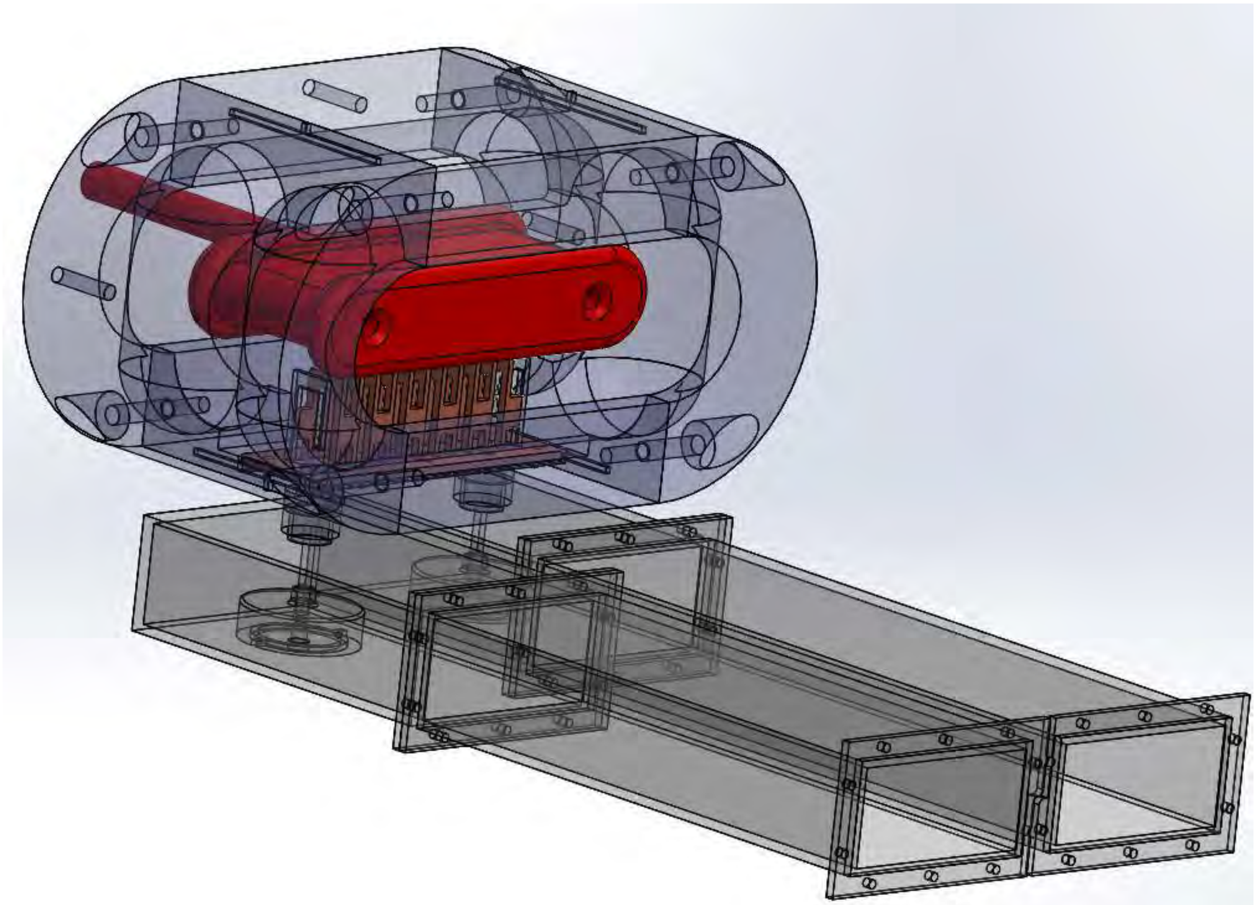

Figure 22: CAD model of the completed RPCFA anode (light gray), slow wave structure (brown), cathode (red), and waveguide extraction system (dark gray).

RPCFA Cold Tests

The completed structure was first cold-tested using a network analyzer, and the results were compared to HFSS simulations, showing good agreement (Figure 23). At the design frequency of 3 GHz, S_{21} was better than -2 dB, and no oscillatory modes were detected within the passband of the amplifier. As expected, the simulated and experimental cold tests determined there was no directionality to the amplifier, with $S_{21} = S_{12}$. Tuning stubs were employed in an attempt to improve the match, but no improvement was observable, suggesting losses were primarily resistive and radiative. While the piece-wise fabrication approach greatly simplified machining and reduced cost, the resulting electrical contacts may lead to increased resistive losses.

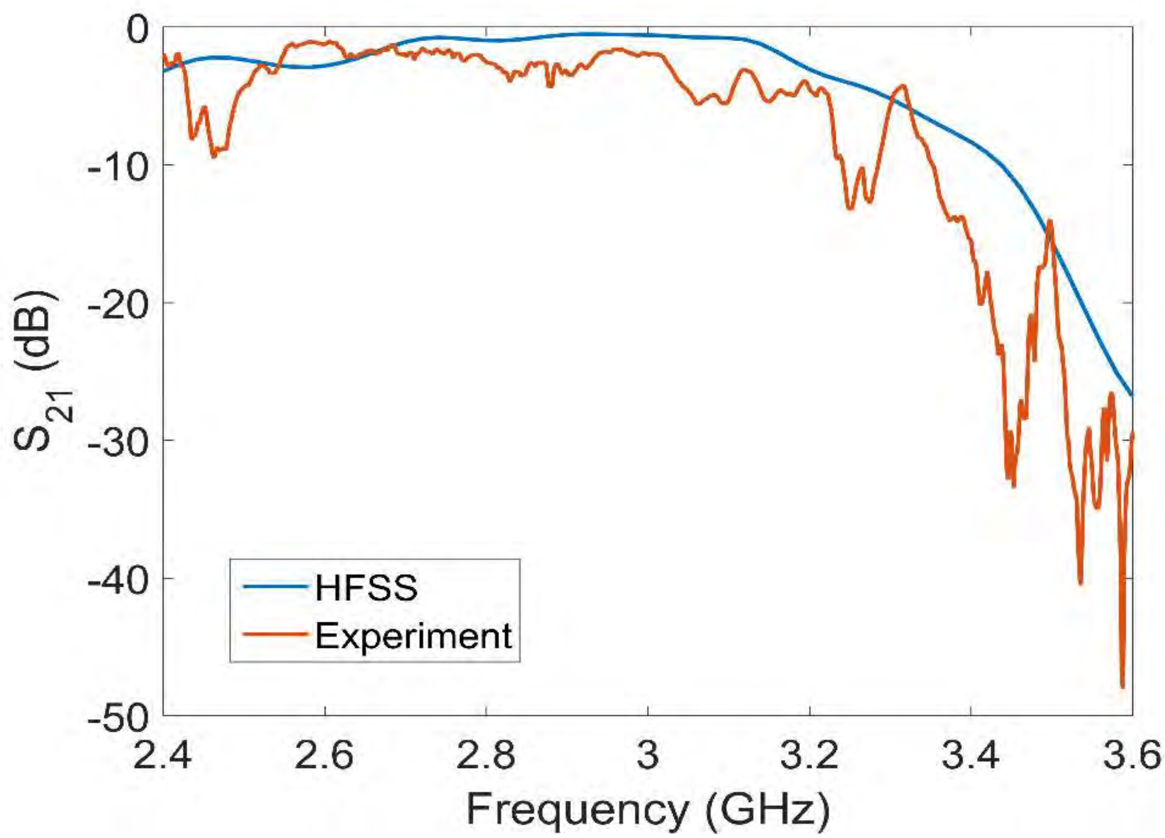

Figure 23: RPCFA cold test results comparing HFSS simulations to experimental measurements.

Zero-Drive Stability

The zero-drive stability of the RPCFA – its failure to oscillate when a pulsed power drive is applied but no RF input is present – was demonstrated first in MAGIC simulations, and then subsequently confirmed in experiments using the Michigan Electron Long Beam Accelerator (MELBA) pulsed power driver. As was the case for all RPCFA testing reported here, MELBA provided a -300 kV, 1-5 kA, ~500 ns drive pulse to the amplifier. As Figure 24 shows, the simulation and experiment are in general agreement, with no significant peaks observed on either spectrum. While it may appear there is a strong oscillation at 3.4 and 4 GHz in Figure 24b, frequencies above 3.95 GHz are over-moded in WR-284 and uncalibrated in these tests. The total peak output power observed on this shot was only 14 W, indicating clear absence of oscillation.

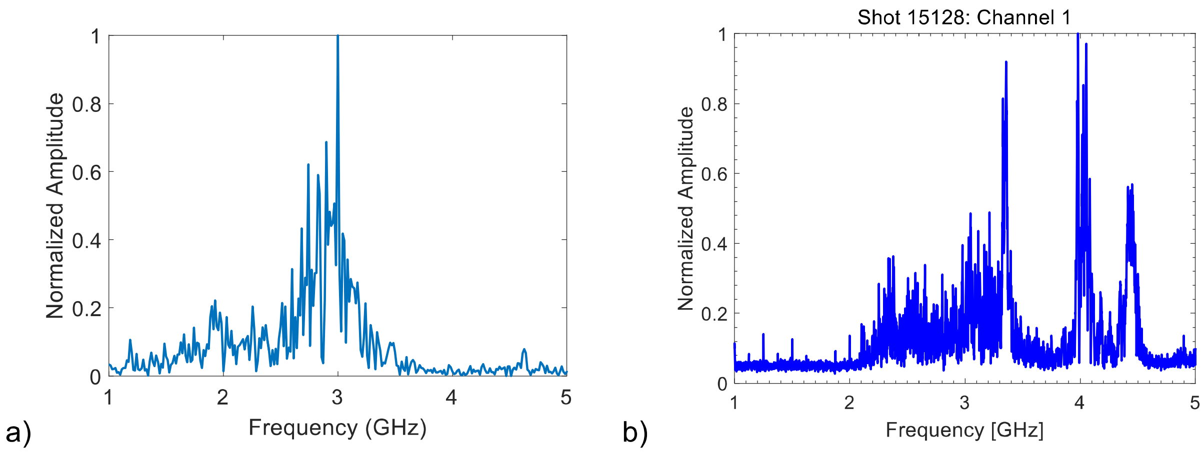

Figure 24: a) Output frequency spectrum of the RPCFA in a MAGIC simulation of the zero RF-drive condition. b) Output frequency spectrum of the RPCFA in an experimental demonstration of the zero RF-drive condition. No significant peaks are observed in either spectrum.

Low & Moderate RF Drive

A 2.835 GHz Raytheon 4J32 capable of 40 kW, and a 3.05 GHz E2V MG5223F capable of 40 kW, were used for the initial tests of the RPCFA. These magnetrons were powered by an existing modulator made by Radiation at Stanford and rated at 40 kV, 30 A for up to 5 μs at 10 kHz. When driving these magnetrons, the highest achievable parameters were ~ 20 kV and 22 A. We typically operated the magnetrons at 182 Hz, with a 5 μs pulselength for the 4J32, and 1 μs pulselength for the MG5223F. As shown in Figure 25, input and reflected power were measured by a directional coupler positioned before the amplifier input, while a second directional coupler measured output power into a resistive load. These signals were split to be directly sampled by a 6 GHz, 20 GS/s oscilloscope, and to make calibrated power measurements using diode detectors.

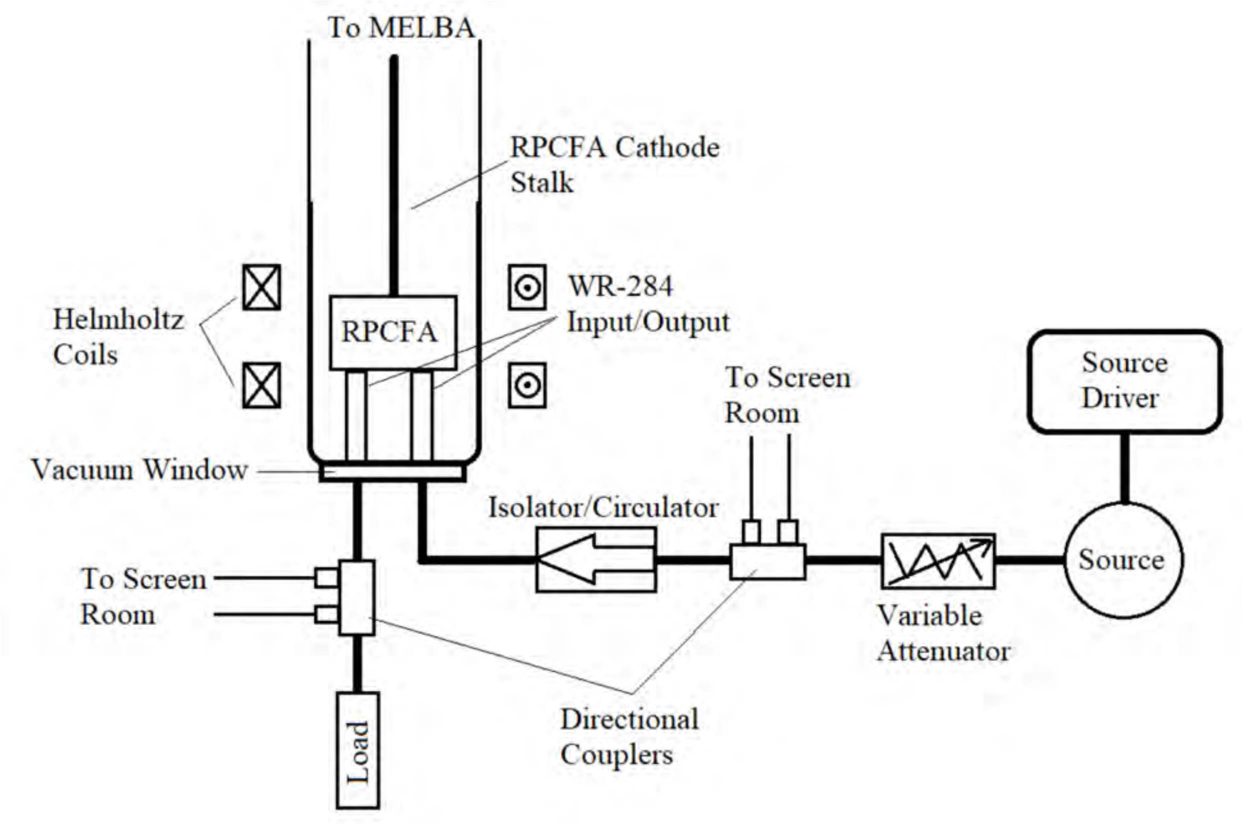

Figure 25: Experimental configuration for RPCFA testing. The isolator and attenuator were not used for the initial experiments.

The initial tests provided many promising results regarding the operation of the RPCFA. Low power tests (~kW), demonstrated the lower edge of the operating band to be 2.63 GHz (Figure 26), an improvement over the 2.7 GHz predicted by simulation.

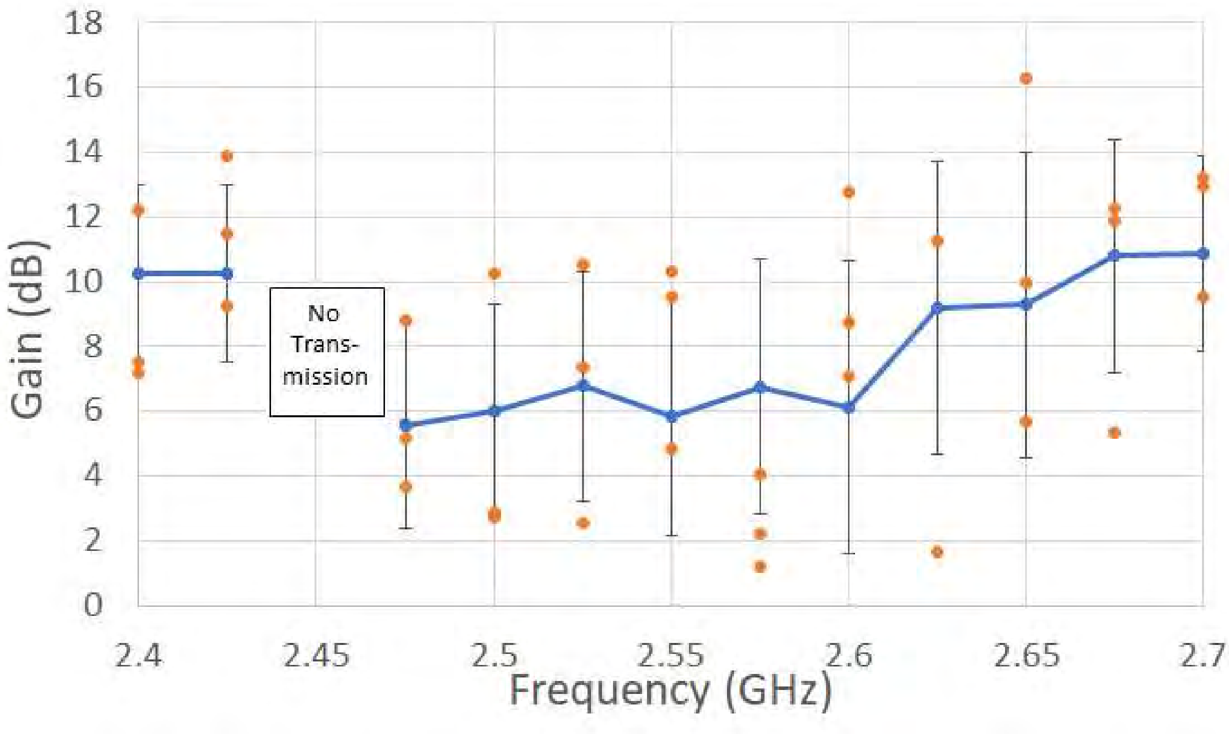

Figure 26: RPCFA bandwidth at low input power, where a reduction in gain is seen below 2.63 GHz. The lower source available was unable to operate above 2.7 GHz.

High spectral purity was observed at 2.84 and 3.05 GHz drive powers (Figure 27).

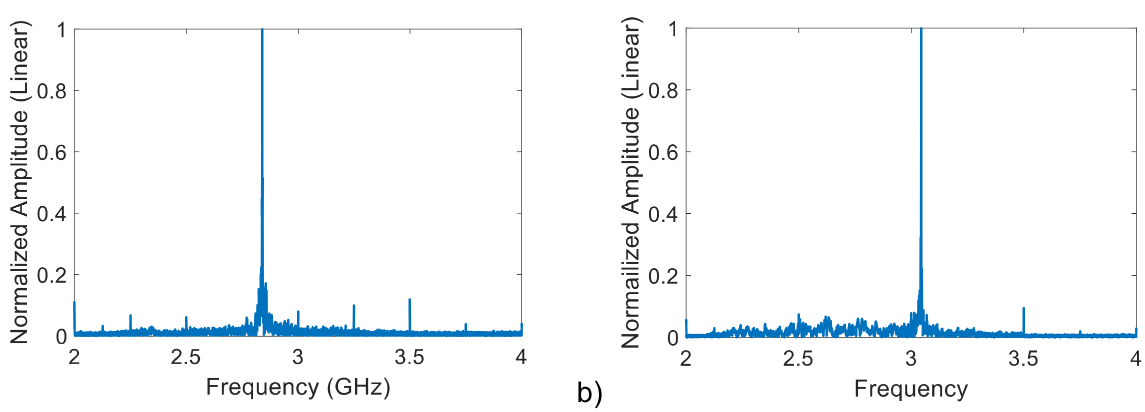

Figure 27: FFT of a RPCFA shot with a) 2.84 GHz RF drive and b) 3.05 GHz RF drive. Both show no evidence of competing modes.

While the gain was somewhat variable at moderate RF drive power (Figure 28), many shots (such as Figure 29) exhibited output powers over 100 kW with RF gain of >10 dB. It was observed that variation in the pulsed power driver was contributing to, but not fully explaining, the variance in RPCFA gain. By filtering out sub-optimal MELBA pulses from the data set the mean gain improved from 6.4 to 6.6 dB, and the standard deviation of the gain improved from

2.7 to 1.6 dB. As we will discuss later, increasing the RF drive was significantly more effective in reducing gain variation.

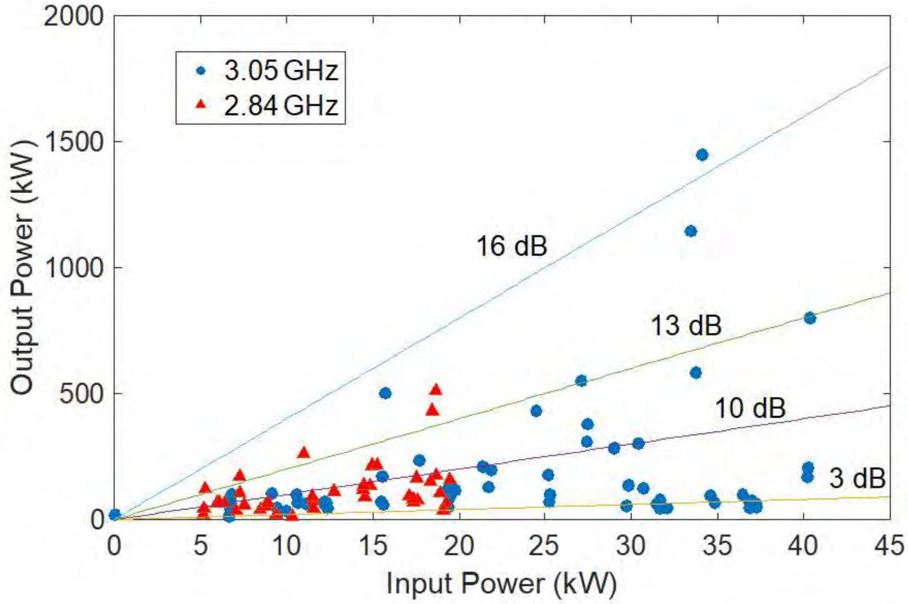

Figure 28: Amplifier gain with both 2.84 and 3.05 GHz RF drive; no data filtering.

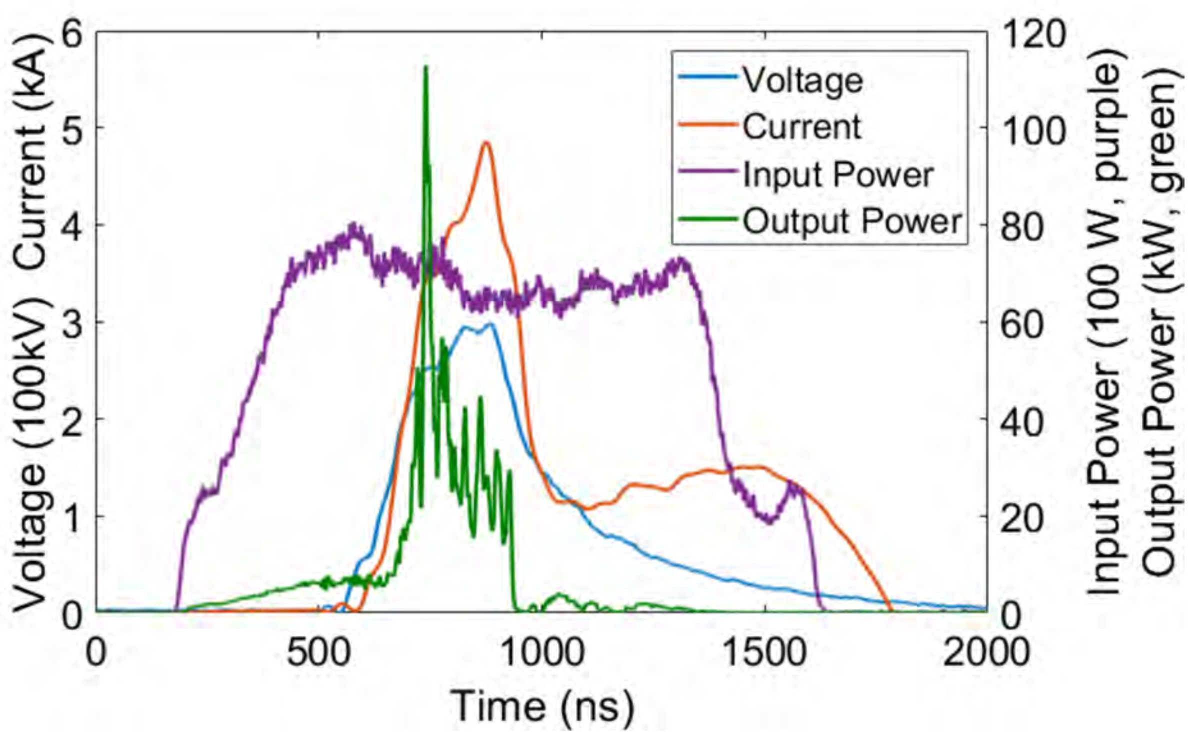

Figure 29: RPCFA shot with 8.5 kW at 3.05 GHz achieved a peak output power of 117 kW for 20 ns (11.7 dB gain).

Cathode Variations

Given the improvements in shot-to-shot consistency that were observed by filtering out variance from the pulsed power driver, we tested a variety of AFRL-fabricated cathodes in an attempt to improve the consistency of MELBA's current generation. Plasma formation from the glyptal-coated aluminum cathode (Figure 30a), was thought to be a possible source of pulse shortening and gain variation in the RPCFA. The Air Force Research Lab was testing a new carbon fiber vendor, and collaborated with UM by brazing a pair of stainless steel cathodes with this material for the RPCFA. Cathode A (Figure 30b) used a coarse brazed carbon emitter, while Cathode B (Figure 30c), used a fine carbon emitter. After testing the initial cathodes, we were concerned with axial current losses, and added an end-cap (Figure 30d) to reduce endloss.

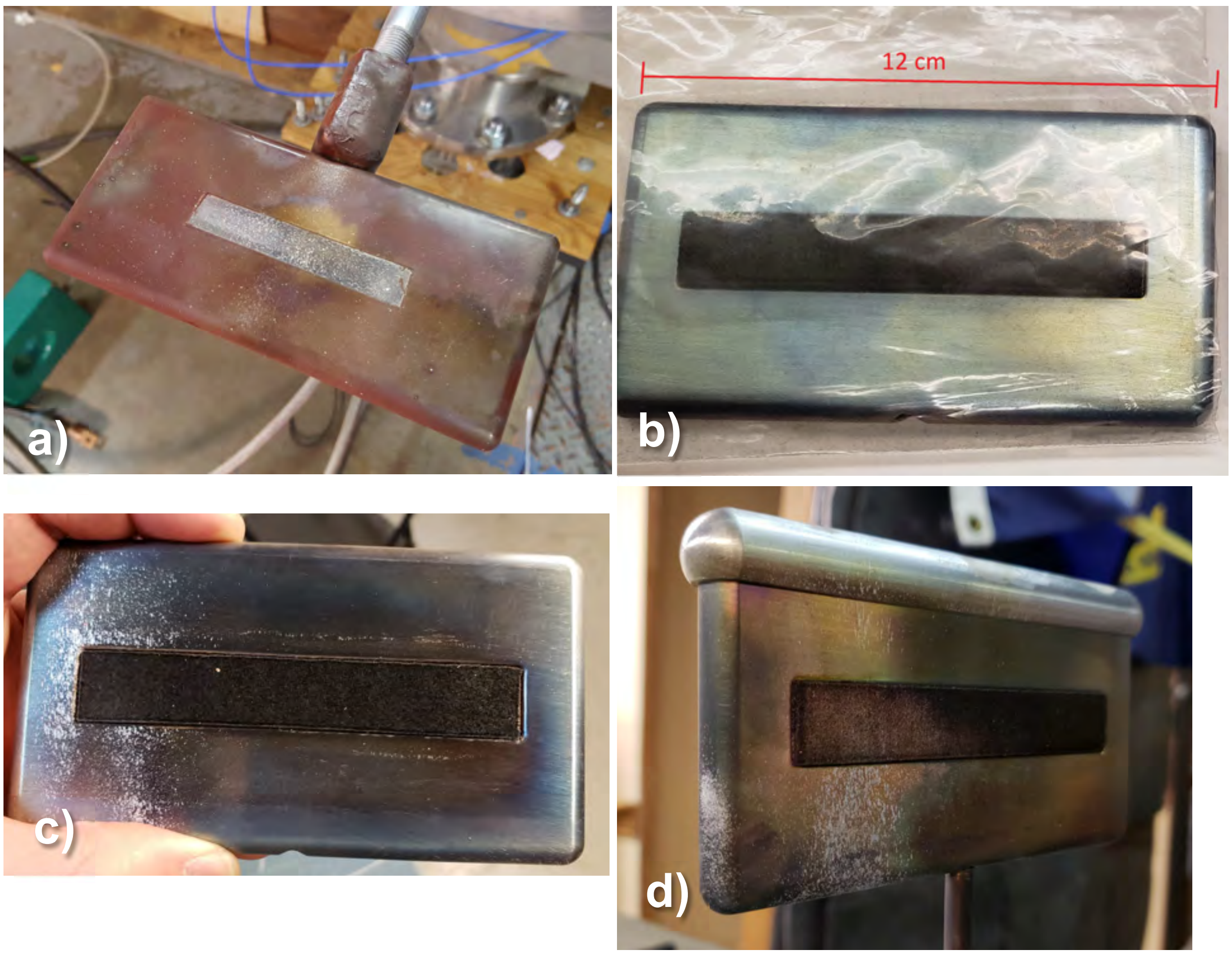

Figure 30: a) original glyptal-coated aluminum cathode with velvet emitter
b) steel cathode with coarse brazed carbon emitter (cathode A)
c) steel cathode with fine carbon emitter (cathode B)
d) cathode A with end-hat

Cathode A, with and without the end-hat, performed comparably to the original glyptal cathode in terms of mean current and amplifier gain, but exhibited reduced shot-to-shot variation (Figure 31). Cathode B also emitted similar current with higher consistency, but produced only half the gain. With more reproducible current, Cathode A was selected for future shots. The results of these cathode tests were included in a joint UM and AFRL publication [14]. It is worth noting that 4 of the AFRL authors on this publication are former members of the UM research group who are now employed at AFRL/RDHP.

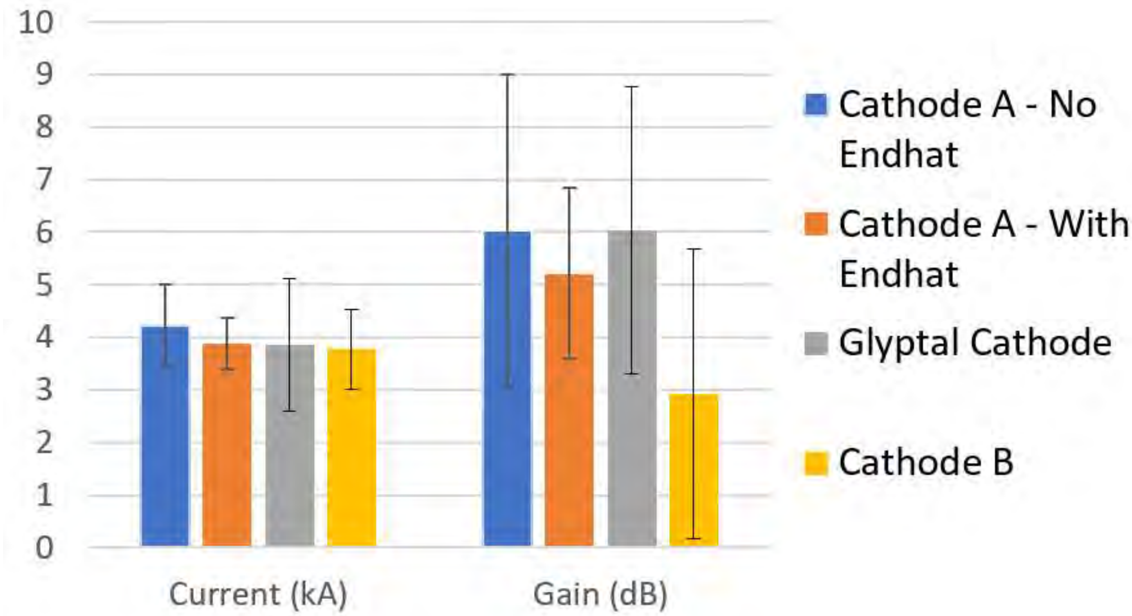

Figure 31: The steel cathode with coarse carbon fiber emitters (cathode A) produced similar current and gain, but demonstrated a reduction in shot-to-shot variation. Cathode B exhibited poor and highly variable performance.

High Power RF Drive

To further improve the reproducibility and performance of the RPCFA, we sought to test it with a MW-level RF input. A set of four 2.6 MW, MG5193 driver magnetrons on hand at UM were selected as the high power source. In order to address concerns about the usability of these magnetrons due to their age, Ph.D. student Steve Exelby collaborated with John Cipolla at L-3 Communications Electron Devices in Williamsport, PA to test two magnetrons on their test stand, validating multi-MW operation (Figure 32).

Additionally, L-3 supplied UM with a solenoid to create an adjustable magnetic field for the MG5193 magnetrons. We had previously used static neodymium magnets calculated (and measured) to produce the correct magnetic field, but we observed during testing at L-3 that a small range of magnetic field tuning from the solenoid was beneficial.

[14] B.W. Hoff, S. Beeson, D. Simon, W. Tang, R. Smith, S.C. Exelby, N.M. Jordan, A. Sayir, R.M. Gilgenbach, P. Lepell, and T. Montoya, "**Brazed Carbon Fiber Fabric Field Emission Cathode**", Review of Scientific Instruments 91, 064702, June 2020.

Figure 32: MG5193 magnetron under test at L-3 Communications. Ch1 (yellow) is the RF output signal. Ch2 (blue) is a Pearson current monitor with a rating of 0.1V/A. Ch3 (purple) is the voltage applied to the cathode. Ch4 (green) is a monitor on the thyratron trigger pulse. Maximum output RF power up to 2 MW was achieved for two magnetrons.

To drive this magnetron at UM, we designed a replacement pulse generator. To accelerate the development process, our colleagues at AFRL sent UM a pulser, but the internals were unfortunately destroyed during transit when a set of capacitors came free from their mount. This chamber and some of its associated hardware, however, were reconfigured to create a custom PFN (Figure 33), demonstrated to deliver a 40 kV, 3 µs pulse into a 400 Ω load.

Figure 33: The eXtra Large Brass (XLB) pulse forming line, with capacitor pairs and air core inductors. Housed within a chamber provided by AFRL, the XLB PFN operates with an atmospheric pressure SF6 fill, producing 40kV for 3 µs into a 400 Ω load.

The MG5193 magnetron, driven by the XLB pulser, expanded the characterization of the RPCFA to RF drive levels above 700 kW (Figure 34). In this regime, the mean gain of the RPCFA improved to 8.8 ± 0.7 dB, but above ~350 kW input (5-6 MW output) the SWS was prone to RF breakdown, limiting the ultimate output power achievable.

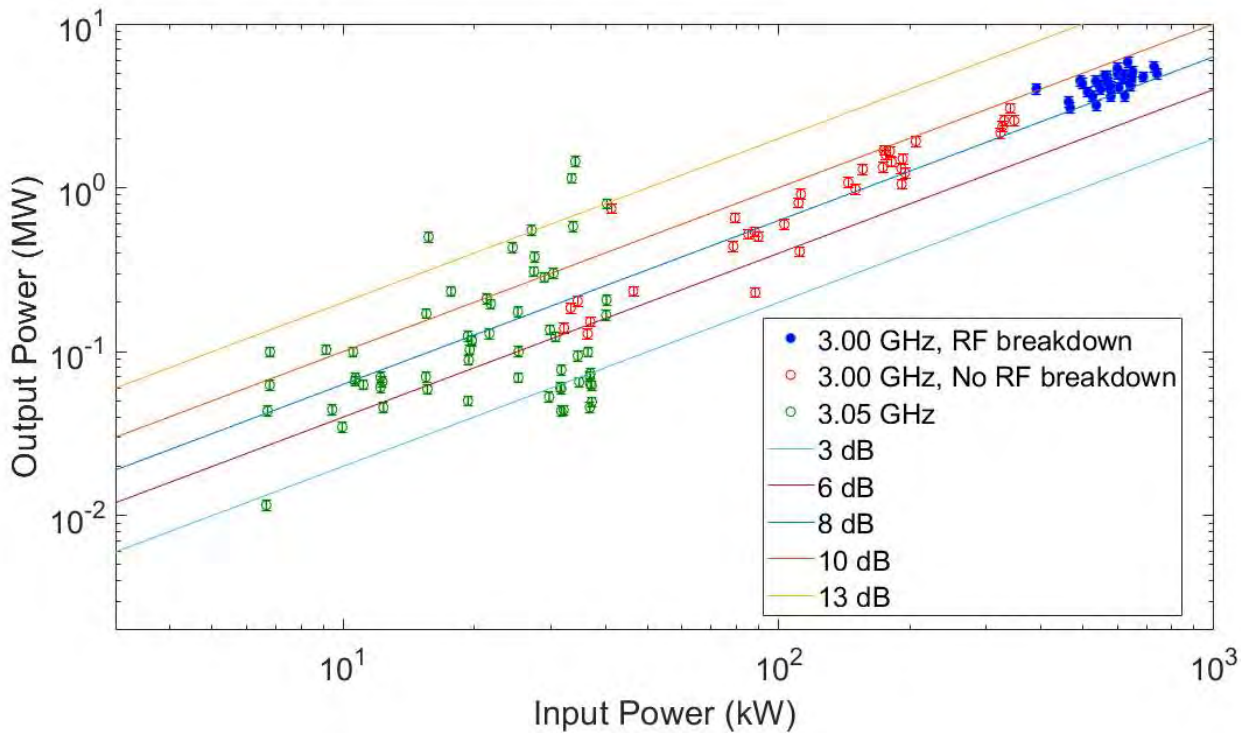

Figure 34: Summary of RPCFA microwave output power versus input power. A transition to reproducible amplification is observed at 150 kW, and RF breakdown becomes an issue above 350 kW input (5-6 MW output).

In Figure 35, we present a shot in which the microwave output power reaches 5 MW, just below the RF breakdown limit of the device. It can be seen that the input signal does not cutoff, indicating that RF breakdown has not occurred.

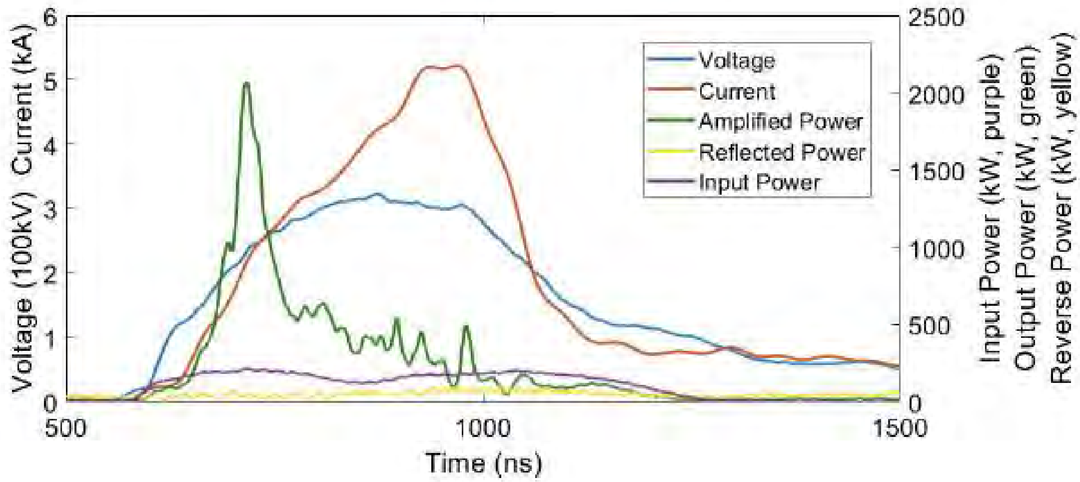

Figure 35: Experimental data traces for RPCFA amplification of microwave input signal at 3.05 GHz; output microwave power signal is 5 MW, just below the RF breakdown limit.

A shot in which RF breakdown has terminated the microwave output is shown in Figure 36. Rapid cutoff of both the microwave output and the input signal indicate that RF breakdown has occurred and shorted out the slow-wave-structure.

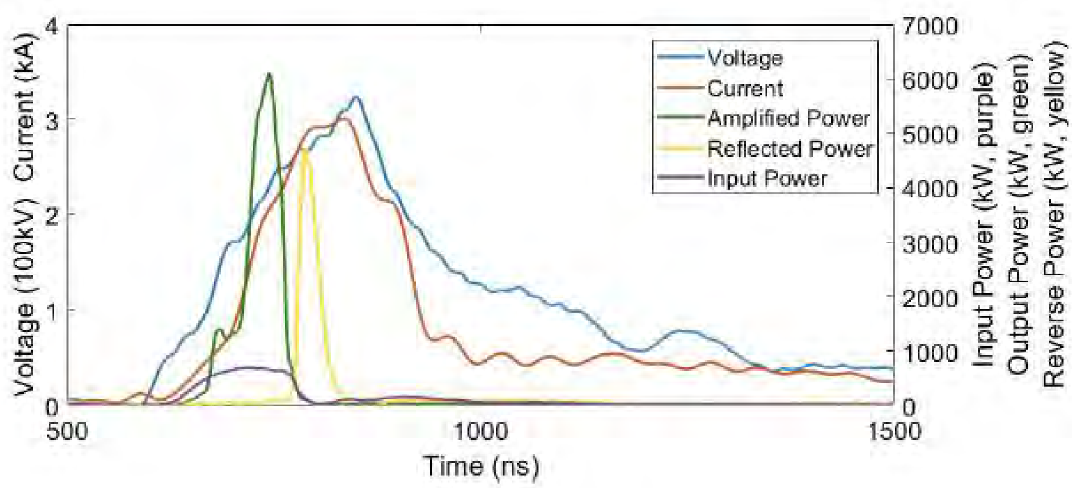

Figure 36: Experimental data traces for RPCFA amplification of 633 kW microwave input signal at 3.0 GHz; output microwave power signal is 5.8 MW, just above the RF breakdown limit.

The complete experimental results of the RPCFA are summarized in Table 2. The RPCFA operates with as little as 100 W RF input, but does not operate consistently until RF input exceeds 150 kW. Beyond 350 kW input (5-6 MW output), RF breakdown within the device limits the output power, though further refinements on the design would likely improve this threshold.

Table 2: Summary of RPCFA response to various input drive power regimes

RF Injected Input Power	0 – 100 W	100 W – 150 kW	150 kW – 350 kW	> 350 kW
Regime	Zero-drive	Irreproducible Amplification	Reproducible Amplification	RF Breakdown
dB Gain (mean ± 1σ)	N/A	7.9 ± 2.7	8.9 ± 0.7	8.8 ± 0.6
Description	Output power is low and no drive frequency is present in the output spectrum.	Output power is highly inconsistent but output frequency is equal to the drive frequency and the spectrum is pure	Output power is predictable and proportional to the input RF power. Spectrum is pure.	Output power is proportional to the input until RF breakdown limits the peak output power.

RPM-CACE

In UM's long-running AFRL collaboration, the Recirculating Planar Magnetron with Coaxial-All-Cavity Extraction (RPM-CACE) was designed under our previous AFOSR research grant (#FA9550-10-1-0104) and fabricated by Air Force Research Lab. The completely RPM-CACE hardware did not arrive at UM until well after the current grant began, so upon conclusion of the RPCFA work we conducted experiments with RPM-CACE (Figure 37).

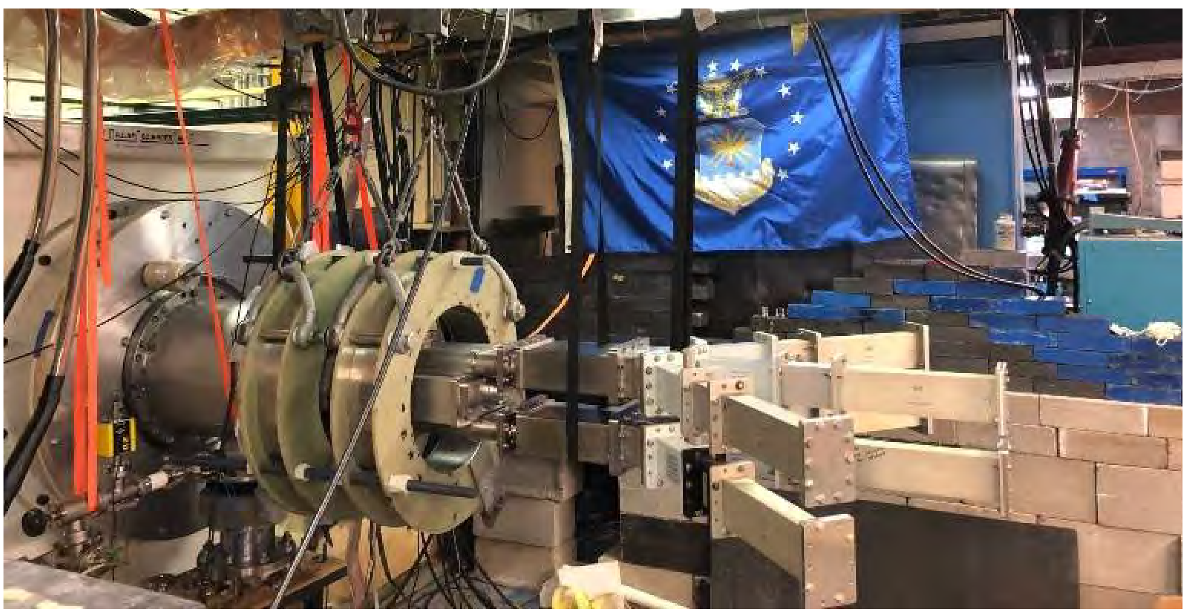

Figure 37: RPM-CACE installed on the MELBA-C driver. Six waveguide directional couplers sample each adjacent pair of the 12 RF cavities.

In simulations conducted at AFRL using ICEPIC, RPM-CACE the design of RPM-CACE was optimized to operate in the π–mode at 1.9 GHz and produce 420 MW with 50-70% efficiency. The key aspect of RPM-CACE, compared to the previously demonstrated RPM-12a [15], is the

[15] M. A. Franzi, "Relativistic Recirculating Planar Magnetrons", Ph.D. dissertation, University of Michigan, Ann Arbor, 2014.

coaxial-all-cavity extraction system to efficiently couple power out of the device [16], and the DFA-340e couplers to make a broadband transition from coaxial to rectangular waveguide (Figure 38).

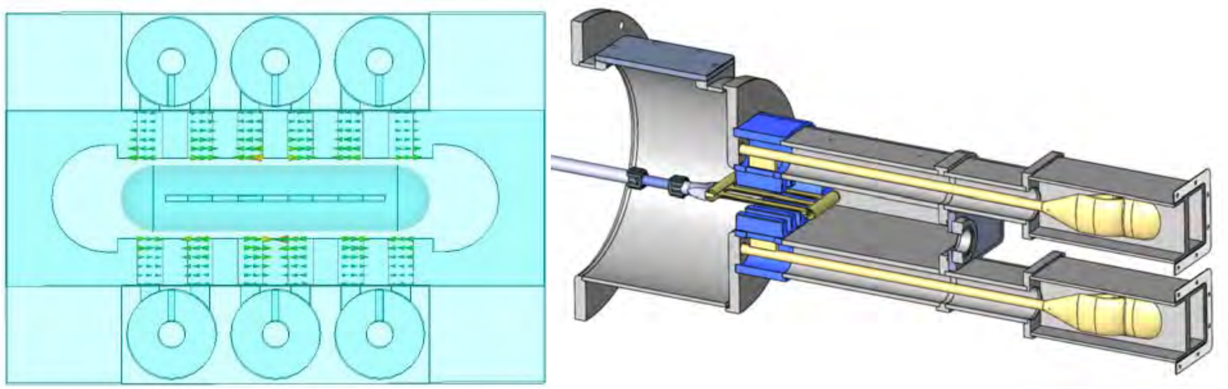

Figure 38: (left) ANSYS model of RPM-CACE showing π-mode electric fields and coaxial all cavity extractors. (right) CAD model cutaway showing transition from of coaxial extractors to rectangular waveguide via DFA-340e couplers.

Calibrated power measurements are made in each waveguide via calibrated directional couplers and HP 8472B diode detectors. Resulting power, current, and power traces for a bare stainless steel cathode are shown in Figure 39.

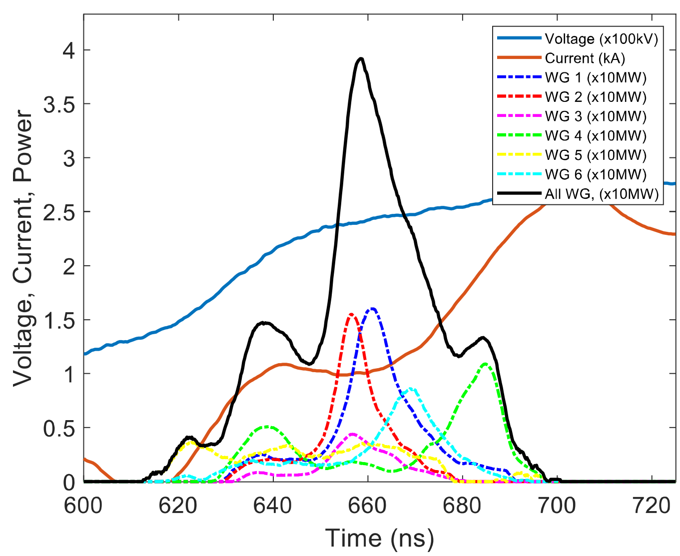

Figure 39: Preliminary experiments of RPM-CACE with a moderate-current, bare stainless steel cathode and a magnetic field of 0.19 T. By sampling all waveguides, we see substantial variation in the timing of peak power in each CACE extractor.

[16] B. W. Hoff, M. Franzi, D. M. French, G. Greening and R. M. Gilgenbach, "A Pi-mode extraction scheme for the axial B-field recirculating planar magnetron," IVEC 2012, Monterey, CA, 2012, pp. 493-494.

The variation in both peak power and time-to-peak power exhibited in Figure 39 suggest that mode competition is occurring within the RPM-CACE. Fast-Fourier Transforms (FFTs) of microwaves in each waveguide arm, shown in Figure 40, support this conclusion, as they have peak frequencies ranging from 1.923 to 1.954 GHz with a lack of spectral purity.

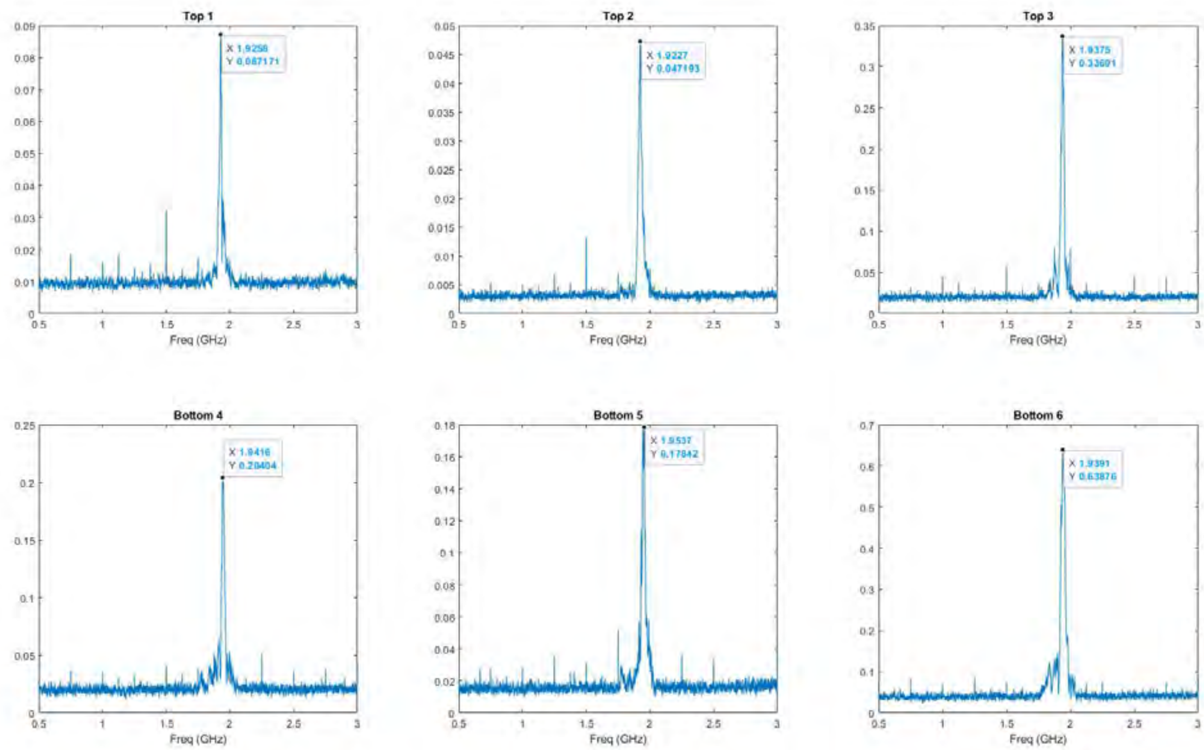

Figure 40: FFT of microwaves in each waveguide arm of the RPM-CACE during a typical shot. Operating frequency varied from 1.923 to 1.954 GHZ, and the width of the peaks indicate mode competition.

Following the initial shot series to validate operation of RPM-CACE, the cathode was removed and shipped to AFRL to be coated via the same carbon fiber fabric process used for the A and B variants of the RPCFA cathode. Unfortunately, research disruptions due to COVID-19 prevented the cathode from being fabricated.

RPM Pulse Shortening

This contract, in conjunction with an AFOSR DURIP grant (#FA9550-15-1-0419), supported research into the evolution of pulse shortening in the RPM. These results were reported in "Ultra-High Speed Framing Camera for Dynamics of High Power Microwave Sources" AFOSR Final Technical Report, December 2016, and will not be repeated here. Please see that report, and its accompanying publication [17], for details.

[17] N.M. Jordan, G.B. Greening, S.C. Exelby, D.A. Packard, Y.Y. Lau, R.M. Gilgenbach, "**Pulse Shortening in Recirculating Planar Magnetrons**", *IEEE Transactions on Electron Devices*, vol. 65, no. 6, pp. 2354-2360, June 2018.

Additively Manufactured HPM Structures

This contract, in conjunction with an AFRL grant (#FA9451-16-1-0050), supported research on the feasibility and durability of additively manufactured structures for high power microwave devices. These results were reported in "Durability Testing of Additively Manufactured High Power Microwave Structures", AFRL-RD-PS-TR-2017-0055, October 2017, and will not be repeated here. Please see that report, and its accompanying publication [18], for details.

Conclusions

We have designed, simulated, fabricated, and characterized a novel crossed-field amplifier concept, the Recirculating Planar Crossed-Field Amplifier (RPCFA). Using HFSS and MAGIC, we designed and optimized the slow-wave structure given the constraints of the available pulsed power system to produce a 3.0 GHz amplifier design with 13.5 dB of gain (29 MW output). In simulation, the amplifier was zero-drive stable and exhibited greater than 50% electronic efficiency, not accounting for electron end-loss. This RPCFA design was fabricated, constructed, and experimentally demonstrated, exhibiting amplification between 2.4 and 3.05 GHz, with peak powers up to 5-6 MW at peak gain of 8-10 dB. Maximum microwave output power was limited by RF breakdown in the slow wave structure, which occurred between 3-6 MW. Amplifier gain exhibited improved reproducibility above 350 kW input microwave power. The RPCFA also demonstrated zero-drive stability in experiments with up to 10 kA of injected current.

Collaborations with AFRL explored the Recirculating Planar Magnetron with Coaxial-All-Cavity Extraction (RPM-CACE). This device was fabricated by AFRL and initial experiments have been performed at UM. Preliminary experiments with low currents from bare metal cathodes have been promising, with total microwave power from all 6-waveguides of some 40 MW. Higher microwave power is expected with carbon fiber cathodes presently being fabricated by AFRL.

Theoretical research has discovered a new space charge parameter, *q*, that describes the modification of the slow-wave circuit mode. This q is analogous to Pierce's original space charge parameter, Q, which describes the modification of the beam mode. This represents a major advancement of Pierce's theory of traveling wave tube amplifier, which has been utilized for some 70 years in various forms. The exact formulation that led to the discovery of q also led to modification of Pierce's gain parameter C and of the Pierce's space charge parameter Q. Most recently, the investigators extended the theory to include the modification of the last Pierce's parameter, the loss parameter, *d*, that accounts all cold-tube circuit loss. In this sense, the modification of Pierce's classical TWT theory is complete.

[18] N. M. Jordan, G. B. Greening, B. W. Hoff, S. S. Maestas, S. C. Exelby and R. M. Gilgenbach, "Additively Manufactured High Power Microwave Anodes," in IEEE Transactions on Plasma Science, vol. 44, no. 8, pp. 1258-1264, Aug. 2016.

Publications

Dissertations

D.H. Simon, “Equilibrium and Stability of Brillouin Flow in Planar, Conventional, and Inverted Magnetrons”, doctoral dissertation, University of Michigan, Ann Arbor, MI, 2016.

P. Y. Wong, “A Contemporary Study in the Theory of Traveling-Wave Tubes,” doctoral dissertation, University of Michigan, Ann Arbor, MI, 2018.

S.C. Exelby, “Design, Development, and Experiments on the Recirculating Planar Crossed Field Amplifier”, doctoral dissertation, University of Michigan, Ann Arbor, 2019.

A. Jassem, “”,doctoral dissertation, University of Michigan, Ann Arbor, 2021. [in progress]

Refereed

Simon, D. H. and Lau, Y. Y. and Greening, G. and Wong, P. and Hoff, B. and Gilgenbach, R. M., “Stability of Brillouin flow in the presence of slow wave structures,” Physics of Plasmas, 23, 092101 (2016).

N. M. Jordan, G. B. Greening, B. W. Hoff, S. S. Maestas, S. C. Exelby and R. M. Gilgenbach, “Additively Manufactured High Power Microwave Anodes,” in IEEE Transactions on Plasma Science, vol. 44, no. 8, pp. 1258-1264, Aug. 2016.

B. W. Hoff, D. S. Simon, D. M. French, Y. Y. Lau, and P. Wong, “Study of a high power sine waveguide traveling wave tube amplifier centered at 8 GHz,” *Physics of Plasmas*, vol. 23, no. 10, p. 103102, Oct. 2016.

D.H. Simon, P. Wong, D. Chernin, Y.Y. Lau, B. Hoff, P. Zhang, C.F. Dong, and R.M. Gilgenbach, “On the evaluation of Pierce parameters C and Q in a traveling wave tube,” *Physics of Plasmas*, vol. 24, no. 3, p. 033114, Mar. 2017.

P.Y. Wong, Y.Y. Lau, D. Chernin, B. Hoff, R.M. Gilgenbach, “Origin of Second Harmonic Signals in Octave Bandwidth Traveling-Wave Tubes,” in *IEEE Transactions on Plasma Science*, vol. 65, no. 2, pp. 710-715, Jan. 2018.

N.M. Jordan, G.B. Greening, S.C. Exelby, D.A. Packard, Y.Y. Lau, R.M. Gilgenbach, “Pulse Shortening in Recirculating Planar Magnetrons”, *IEEE Transactions on Electron Devices*, vol. 65, no. 6, pp. 2354-2360, June 2018.

S. C. Exelby, G.B. Greening, N.M. Jordan, D.A. Packard, D.H. Simon, Y.Y. Lau, B.W. Hoff, R.M. Gilgenbach, “High-Power Recirculating Planar Crossed-Field Amplifier Design and Development,” *IEEE Transactions on Electron Devices*, vol. 65, no. 6, pp. 2361-2365, June 2018.

F. Antoulinakis, P. Wong, A. Jassem, and Y. Y. Lau, “Absolute instability and transient growth near the band edges of a traveling wave tube“, *Physics of Plasmas,* 25, 072102 July 2018.

P.Y. Wong, D. Chernin, and Y.Y. Lau, "Modification of Pierce's Classical Theory of Traveling-Wave Tubes," *IEEE Electr. Dev. Lett.* 39 1238-1241 (2018).

A. Jassem, P. Y. Wong, D. P. Chernin, Y. Y. Lau, F. Antoulinakis, D. Packard, T. A. Hargreaves and C. M. Armstrong, "Extensions of Johnson's Theory of Backward Wave Oscillations in a Traveling Wave Tube," IEEE Transactions on Electron Devices 66, 1519-1524 (2019).

A. Jassem, Y. Y. Lau, D. P. Chernin, and P. Wong, "Theory of traveling wave tube including space charge effects on the circuit mode and distributed cold tube loss," IEEE Transactions on Plasma Science 48, 665-668 (2020).

B.W. Hoff, S. Beeson, D. Simon, W. Tang, R. Smith, S.C. Exelby, N.M. Jordan, A. Sayir, R.M. Gilgenbach, P. Lepell, and T. Montoya, "Brazed Carbon Fiber Fabric Field Emission Cathode", Review of Scientific Instruments 91, 064702 (2020).

S.C. Exelby, G.B. Greening, N.M. Jordan, D.A. Packard, D. Simon, Y.Y. Lau, B.W. Hoff, R.M. Gilgenbach, "High-Power Amplification Experiments on a Recirculating Planar Crossed-Field Amplifier", in IEEE Transactions on Plasma Science, vol. 48, no. 6, pp. 1917-1922, June 2020.

Conference Presentations

N. Jordan, G. Greening, S. Exelby, R. Gilgenbach, Y. Lau, B. Hoff, "3-D Printed High Power Microwave Magnetrons", 15th APS-DPP, Savannah, GA, November 2015.

N. Jordan, G. Greening, S. Exelby, R. Gilgenbach, Y. Lau, B. Hoff, "Additively Manufactured Anodes in a Relativistic Planar Magnetron", IVEC 2016, Monterey, CA, April 2016.

N. Jordan, G. Greening, S. Exelby, R. Gilgenbach, Y. Lau, B. Hoff, "Recent Experiments on the Recirculating Planar Magnetron", IPMHVC 2016, San Jose, CA, July 2016. **[Invited]**

N. Jordan, G. Greening, S. Exelby, R. Gilgenbach, Y. Lau, B. Hoff, S. Maestas, "Additively Manufactured Structures for High Power Microwave Devices", ICOPS 2016, Banff, CA, June 2016. **[Invited]**

S. Exelby, G. Greening, N. Jordan, D. Simon, Y. Y. Lau, R. Gilgenbach, and B. Hoff, "Design and Simulation of the Recirculating Crossed-Field Planar Amplifier," Bulletin of the American Physical Society-DPP, Nov. 2016.

N. M. Jordan, G. B. Greening, S. C. Exelby, D. A. Packard, K. A. Schneider, Y. Y. Lau, and R. M. Gilgenbach, "Pulse Shortening in Recirculating Planar Magnetrons", IVEC, London, UK, April 2017. **[Invited]**

N. M. Jordan, G. B. Greening, S. C. Exelby, D. A. Packard, K. A. Schneider, Y. Y. Lau, R. M. Gilgenbach, "Plasma-Based Pulse Shortening in the Recirculating Planar Magnetron", ICOPS, Atlantic City, NJ, May 2017.

S. C. Exelby, G. B. Greening, N. M. Jordan, D. Simon, Y. Y. Lau, R. M. Gilgenbach, B.W. Hoff, "Design and Development of the Recirculating Planar Crossed-Field Amplifier", ICOPS, Atlantic City, NJ, May 2017.

S.C. Exelby, G.B. Greening, N.M. Jordan, D.A. Packard, Y.Y. Lau, R.M. Gligenbach, D.H. Simon, and B.W. Hoff, "Design, Simulation and Experiments on the Recirculating Crossed-Field Planar Amplifier", *APS-DPP*, Milwaukee, WI, October 2017.

N. M. Jordan, G. B. Greening, D. A. Yager-Elorriaga, A.M. Steiner, S.C. Exelby, P.C. Campbell, D.A. Packard, S.R. Miller, J.M. Woolstrum, S.V. Langellotti, N.B. Ramey, A.P. Shah, Y.Y. Lau, R.D. McBride, and R.M. Gilgenbach, “Facility Upgrades and Recent Experimental Work at the University of Michigan”, IPMHVC 2018, Jackson Hole, WY, June 2018. **[Invited]**

S.C. Exelby, G.B. Greening, N.M. Jordan, D.A. Packard, D.H. Simon, Y.Y. Lau, R.M. Gligenbach, and B.W. Hoff, "Microwave Gain in a Recirculating Planar Crossed-Field Amplifier", *IVEC 2018*, Monterey, CA, April 2018.

S.C. Exelby, G.B. Greening, N.M. Jordan, D.A. Packard, Y.Y. Lau, R.M. Gilgenbach, "Experimental Microwave Gain Measurements on a Recirculating Planar Crossed-Field Amplifier", ICOPS 2018, Denver, CO, June 2018.

S. C. Exelby, G. B. Greening, N. M. Jordan, D. A. Packard, Y. Ying Lau and R. M. Gilgenbach, “Experiments and Simulations of the Recirculating Planar Crossed-Field Amplifier”, 60th APS-DPP, Portland, OR, Nov 2018.

S.C. Exelby, G.B. Greening, N.M. Jordan, D.A. Packard, Y.Y. Lau, and R.M. Gilgenbach, “Experiments on a Recirculating Planar Crossed-Field Amplifier”, IVEC 2019, Busan, South Korea, April 2019.

S.C. Exelby, G.B. Greening, N.M. Jordan, D.A. Packard, Y.Y. Lau, R.M. Gilgenbach, B.W. Hoff, D.H. Simon, "High Power Amplification Experiments on a Recirculating Planar Crossed Field Amplifier", ICOPS 2019, Orlando, FL, June 2019.

R.M. Gilgenbach, S. Exelby, D. Packard, C. Swenson, B. Sporer, N. Jordan, R. McBride, Y.Y. Lau, "Crossed-Field, High Power Microwave Oscillators and Amplifiers", Pacific Symposium on Pulsed Power and Applications, Kuaui, Hawaii, August 2019.

S.C. Exelby, N.M. Jordan, D.A. Packard, Y.Y. Lau, R.M. Gilgenbach, B.W. Hoff, D.H. Simon, “Multi-MW Output from the Recirculating Planar Crossed-Field Amplifier”, 61st APS-DPP, Ft. Lauderdale, FL, Oct 2019.

B.W. Hoff, F. Hegeler, S. Beeson, M.C. Myers, D. Simon, W. Tang, R. Smith, S. Exelby, N.M. Jordan, A. Sayir, R.M. Gilgenbach, "Brazed Carbon Fiber Fabric Field Emission Cathodes", IPMHVC 2020, Knoxville, TN, May 2020. [cancelled]

N.M. Jordan, D.A. Packard, S.C. Exelby, P.C. Campbell, B.J. Sporer, A.P. Shah, G.V. Dowhan, T.J. Smith, C.J. Swenson, Y.Y. Lau, R.D. McBride, R.M. Gilgenbach, "High Power Microwave and Pulsed Power Development at the University of Michigan", IPMHVC 2020, Knoxville, TN, May 2020. [Invited] [cancelled]

N.M. Jordan, C.J. Swenson, D.A. Packard, M.A. Franzi, B.W. Hoff, S. Tummala, Y.Y. Lau, R.M. Gilgenbach, “Initial Experiments on the Recirculating Planar Magnetron with Coaxial All-Cavity Extraction”, ICOPS 2020, Dec 2020.

Personnel Support

Research Scientists supported on this grant: N.M. Jordan and P. Zhang

Students supported on this grant: Graduate Students: D.H. Simon, P. Wong, A. Jassem, S. Exelby, D. Packard, S. Tummala, C. Swenson

Undergraduate Students involved: Emma Guerin